Review

CONTRAST MEDIA & MOLECULAR IMAGING

Received: 22 October 2008, Revised: 5 December 2008, Accepted: 7 December 2008, Published online in Wiley InterScience: 2009

(www.interscience.wiley.com) DOI:10.1002/cmmi.265

Classification and basic properties of contrast agents for magnetic resonance imaging

Carlos F. G. C. Geraldes[a]* and Sophie Laurent[b]

A comprehensive classification of contrast agents currently used or under development for magnetic resonance imaging (MRI) is presented. Agents based on small chelates, macromolecular systems, iron oxides and other nanosystems, as well as responsive, chemical exchange saturation transfer (CEST) and hyperpolarization agents are covered in order to discuss the various possibilities of using MRI as a molecular imaging technique. The classification includes composition, magnetic properties, biodistribution and imaging applications. Chemical compositions of various classes of MRI contrast agents are tabulated, and their magnetic status including diamagnetic, paramagnetic and superparamagnetic are outlined. Classification according to biodistribution covers all types of MRI contrast agents including, among others, extracellular, blood pool, polymeric, particulate, responsive, oral, and organ specific (hepatobiliary, RES, lymph nodes, bone marrow and brain). Various targeting strategies of molecular, macromolecular and particulate carriers are also illustrated. Copyright © 2009 John Wiley & Sons, Ltd.

Keywords: lanthanide complexes; contrast agents; magnetic resonance imaging

1. INTRODUCTION

Magnetic resonance imaging (MRI) is based on the principles of nuclear magnetic resonance (NMR) spectroscopy, whereby images are generated by spatially encoding the NMR signal coming from nuclei (e.g. protons) present in the object to be imaged through the application of time-varying, linear magnetic field gradients (1). A very high spatial resolution and the ability to distinguish soft tissues are the main advantages of MRI. However, sometimes insufficient contrast is observed and, thus, the use of contrast agents (CAs) is of great assistance in many applications of MRI. A number of such substances have been developed and research continues in order to find more selective contrast media that will allow a better delineation of diseases, thus helping radiologists to make a more precise diagnosis. We describe below the different classes of CAs and give some examples, providing an overview not only of current clinical CAs, CAs undergoing clinical evaluation and compounds following new ideas, but also of some of their applications.

Currently available MR CAs can be classified in different ways, according to their various features, such as (a) the presence and nature of their metal center, (b) their magnetic properties, (c) their effect on the image, (d) their chemical structure and ligands present or (e) their biodistribution and applications. As several of these items are intimately related, and in order to avoid unnecessary repetition, here we will simplify the above classification. We will start by using together the criteria of the CAs chemical composition (including metal center and ligands present), the resulting magnetic properties and the corresponding effects on the MRI image. Then, the biodistribution and the resulting applications of the CAs will be used as an alternative classification approach (2–9).

2. CHEMICAL COMPOSITION, MAGNETIC PROPERTIES AND EFFECT ON THE IMAGE

2.1. Chemical composition

The chemical composition of CAs varies widely (2–9). They can be small mononuclear or polynuclear paramagnetic chelates; metalloporphyrins; polymeric or macromolecular carriers (covalently or noncovalently labeled with paramagnetic chelates); particulate CAs (including fluorinated or nonfluorinated paramagnetic micelles or liposomes) and paramagnetic or superparamagnetic particles (e.g. iron oxides, Gd^{3+}-labeled zeolites); diamagnetic CEST polymers; diamagnetic hyperpolarization probes (gases and aerosols), and ^{13}C-labeled compounds or ions (e.g. $6Li^{+}$).

With regards to the metal center, the simplest one is a single paramagnetic ion bound to an organic ligand in a chelate. The paramagnetic ion is usually Gd^{3+} or Mn^{2+} for simple paramagnetic relaxation agents, and the most common ligands are

* *Correspondence to: C. F. G. C. Geraldes, Department of Biochemistry, Faculty of Science and Technology, University of Coimbra, P-3001-401 Coimbra, Portugal. E-mail: geraldes@bioq.uc.pt*

a *C. F. G. C. Geraldes*
Department of Biochemistry, Faculty of Science and Technology, and Center of Neurosciences and Cell Biology, University of Coimbra, P-3001-401 Coimbra, Portugal

b *S. Laurent*
NMR and Molecular Imaging Laboratory, Department of General, Organic and Biomedical Chemistry, University of Mons-Hainaut, B-7000 Mons, Belgium

Biographies

Carlos F. G. C. Geraldes has been Professor of Chemistry and Biochemistry at the University of Coimbra, Portugal, since 1988. He is Director of the NMR Laboratory of the Center of Neurosciences and Cell Biology at the University of Coimbra. He was a representative of Portugal in the European Union COST Chemistry Technical Committee between 1994 and 2001. The author of more than 200 original research papers, he was awarded the prize of Excellence in Research from the Portuguese Fundação para a Ciência e Tecnologia in 2004. His present interests include targeted contrast agents for molecular imaging.

Sophie Laurent received her PhD in Chemistry in 1993 and is currently Lecturer at the University of Mons-Hainaut, Belgium. She is the leader of the Chemical Synthesis Team of the General, Organic and Biomedical Chemistry Laboratory. The author of more than 60 original research papers, her present interests include vectorization of contrast agents for molecular imaging.

linear or macrocyclic polyaminocarboxylate/phosphonate derivatives (see below). Other paramagnetic agents include a small number of nonmagnetically coupled ions bound to small chelates, or a large number of Gd^{3+} chelates bound to polymeric carriers such as dendrimers or proteins.

Gd^{3+} ions are also used in many particulate CAs, such as bound to amphiphylic chelates in paramagnetic micelles, in the bilayer of liposomes, as small chelates in their aqueous internal compartment, bound to porous materials like zeolites, or bound in gadolinium oxide nanoparticles. Iron is frequently used in a variety of iron oxide particles of different sizes and coatings (see below) (8).

Paramagnetic chelates containing Ln^{3+} ions (such as Dy^{3+} or Tm^{3+}) can be used as MRI CAs in different ways. For instance, as susceptibility agents, when they are in a compartment, affecting T_2 or T_2^* relaxation (10), or as PARACEST and LIPOCEST agents, where the paramagnetic shift effect of the ion on the proton nuclei of the CA facilitates the irradiation of their shifted resonances and the consequent saturation transfer by chemical exchange (CEST effect), thus decreasing the water proton signal intensity and leading to a negative image contrast (see below) (9).

Less conventional MRI CAs may not contain a metal center at all. These include diamagnetic agents, such as oral agents or the CEST agents initially proposed. Another family of agents recently used in MRI are the dynamic nuclear polarization (DNP) agents, such as hyperpolarized noble gases (^3He, ^{129}Xe) and ^{13}C-labeled organic compounds or ions like $^6Li^+$. The strong signal enhancement from the probe's nuclei with long T_1 values allows the direct imaging of the probe's molecular distribution (a kind of positive contrast), thus making this MRI technique similar (and competitive) to other molecular imaging techniques such as positron emission tomography (PET).

2.2. Magnetic properties and image effects

CAs can also be classified according to their magnetic properties as paramagnetic or superparamagnetic agents.

2.2.1. *Paramagnetic agents*

Metal ions with one or more unpaired electrons are paramagnetic, and therefore possess a permanent magnetic moment. Organic free radicals are also paramagnetic because of their unpaired valence electron. In aqueous solution, there is a dipolar magnetic interaction between the electronic magnetic moment of the paramagnetic atom and the much smaller magnetic moments of the protons of the nearby water molecules. Molecular motions cause random fluctuations in this dipolar magnetic interaction, reducing both the longitudinal (T_1) and the transverse (T_2) relaxation times of the water protons. Gadolinium (Gd^{3+}) and manganese (Mn^{2+}) are examples of paramagnetic ions which are used as MR CAs, because their physical properties are suitable for efficiently reducing the T_1 and T_2 proton relaxation times. They possess, respectively, seven or five unpaired electrons and symmetrical (^8S or ^6S) ground states, resulting in slower electronic spin relaxation rates. The relaxation theory of paramagnetic systems has been extensively described in the literature (11,12).

Paramagnetic metal ions, like Gd^{3+}, cannot be used as CAs in their ionic form due to their undesirable biodistribution (accumulating in bones, liver or spleen) and relatively high toxicity. Gd^{3+} undergoes a rapid hydrolysis at physiological pH, producing insoluble $Gd(OH)_3$. Thus, metal ion complexes (chelates) with a high thermodynamic and kinetic stability are required for the use of these paramagnetic metal ions *in vivo*, giving appropriate biodistribution and safety profiles.

MR CAs work by reducing the T_1 and T_2 relaxation times of nuclei in the target tissue, and are thus described as either 'T_1 agents' or 'T_2 agents' depending on whether the relative reduction in relaxation times caused by the CA is greater for T_1 or T_2. The efficiency of MRI CAs is measured in terms of their r_1 and r_2 *relaxivity* values, which indicate their ability to decrease, respectively, the T_1 and T_2 relaxation times of the water protons per unit (mM) concentration of metal ion. The contrast enhancement is obtained when one tissue has either higher affinity for the CA or higher vascularity than another one. Diseased tissues, such as tumors, are metabolically different from healthy tissues and have a much higher uptake of the CAs, resulting in a higher contrast in MRI images. T_1-weighted images give positive image contrast, as the image signal intensity increase at the tissue site where the CA concentrates is dominated by T_1 shortening. T_2-weighted images give negative contrast, due to the predominant effect of T_2 shortening. The

small Gd^{3+} or Mn^{2+}-based paramagnetic chelates present in nonspecific CAs have similar r_1 and r_2 effects in water, and are currently used mainly for positive contrast T_1-weighed images. The relaxivity effects of these agents result mostly from both inner- and outer-sphere mechanisms (2–5,7).

2.2.2. *Superparamagnetic agents*

These agents consist of materials, such as iron oxides, in the form of colloids made up of particles (typically 5–200 nm in diameter) in suspension, which are composed of very small crystallites (1–10 nm) containing several thousand magnetic ions. For these agents, the thermal energy below the Curie or Neel temperature, although it may not be sufficient to overcome the coupling forces between neighboring atoms, is sufficient to change the direction of the magnetization of the entire crystallite. The resulting fluctuations in the direction of the magnetization cause the internal magnetic field to average to zero. The superparamagnetic material behaves similarly to paramagnetism, except that, instead of each individual atom being independently influenced by an external magnetic field, the magnetic moment of the entire crystallite tends to align with that magnetic field. Thus, the magnetic moments of the individual ions do not cancel out but are mutually aligned, and the crystallites have a permanent magnetic moment, which is very large in the presence of a magnetic field, much larger than that of a single molecule of a Gd chelate (8,13).

Each of these particles is made of a core of one or more magnetic crystallites embedded in a coating, made for example from dextrans (in ferumoxide) or siloxanes (in ferumoxsil), which prevents agglomeration. The crystallites are made up of nonstoichiometric iron oxides. The dimension of the core determines the particle relaxivities, while that of the overall particle governs its pharmacokinetics.

There are three kinds of particulate superparamagnetic iron oxides, according to the overall size of the particles: (a) if they have a diameter $d < 50$ nm, they are known as ultra-small superparamagnetic iron oxide (USPIO) particles; (b) if $1\ \mu m > d > 50$ nm, they are called small superparamagnetic iron oxide (SPIO) particles; and (c) micron-sized particles of iron oxide (MPIO) are large particles, with a diameter of several microns. While the overall size of the former two classes allows intravenous administration, the large particles can only be administered orally to explore the gastrointestinal tract; otherwise they would be trapped in the lung alveoli. Some MPIOs are also used to visualize individual cells. SPIOs can be used as negative CAs for liver imaging, as they are taken up by phagocytic–endocytic systems, such as the reticuloendothelial system (RES) of the liver (Kupffer cells) and the spleen. Particles with a diameter of less than 300 nm remain intravascular for a prolonged period of time and thus can serve as blood pool agents. There are still other formulations, such as monocrystalline iron oxide particles (MION) and cross-linked iron oxides (CLIO).

The relaxation induced by superparamagnetic particles (13) can be explained by the classical outer-sphere relaxation theory, reformulated by the Curie relaxation theory (14). The outer-sphere relaxation theory considers the relaxation rates of water protons diffusing nearby the unpaired electrons responsible for the particle's magnetization (15). These agents exhibit strong T_1 relaxation properties, and due to susceptibility differences to their surroundings, also produce a strongly varying local magnetic field, which enhances T_2 relaxation. An important result from the outer-sphere theory is that the r_2/r_1 ratio increases with increasing particle size, and thus smaller particles are much better T_1-shortening agents than larger ones (16–18). As a consequence of their larger size and magnetic moment, SPIOs were initially developed as T_2-agents, producing a dark area on MRI images resulting from their negative contrast effect (19). However, a new generation of USPIOs, with sizes less than 10 nm, has also been reported to have excellent T_1-enhancing properties (17,18,20,21).

Iron oxide-based CAs currently in clinical use are summarized in Table 1, while their properties and applications are described in Tables 3–5.

2.2.3. *Susceptibility agents*

On a more macroscopic scale, long-range interactions can dominate T_2 or T_2^* relaxation for all types of CAs. This relaxation mechanism, known as susceptibility-induced relaxation (10), is

Table 1. Iron oxide based MR contrast agents in current clinical use

USPIOs

- Sinerem® (Guerbet), also called Combidex®, ferumoxtran and AMI-227 (AMAG Pharmaceuticals), have crystal diameters of 4.3–4.9 nm and overall diameters of about 50 nm, with r_1 and r_2 of 22.7 and 53.1/mM/s, respectively, at 20 MHz and 37°C (22).
- Clariscan® or PEG-FERRON (GE Healthcare), an intravascular agent (23).

SPIOs

- Endorem™ (Guerbet), also called Feridex®, ferumoxide and AMI-25 (AMAG Pharmaceuticals) (24), composed of nonstoichiometric magnetite crystals of radius 4.3–4.8 nm, average particle diameter of about 200 nm, with r_1 and r_2 of 24 and 107/mM/s, respectively, at 20 MHz and 37°C (22).
- Resovist® (Bayer Schering Pharma AG), suspension of nanoparticles of magnetite and maghemite coated with carboxydextran; the core contains several crystals each with diameter of about 4.2 nm, and overall particle diameter of around 62 nm, and r_1 and r_2 of 20 and 190/mM/s, respectively, at 20 MHz and 37°C (25,26).

Large particles for oral administration

- Abdoscan® (GE Healthcare), composed of monodisperse polymer particles of 3 μm diameter coated with crystals of iron oxide (27,28).
- Lumirem® (Guerbet), also called ferumoxsil, AMI-121 and GastroMARK® (AMAG Pharmaceuticals), a silicone-coated superparamagnetic iron oxide suspension.

related to the magnetization of the CA, which results from the partial alignment of the individual magnetic moments in the direction of the magnetic field. When a CA becomes compartmentalized, such as when superparamagnetic particles are taken up by Kupffer cells, or in a vessel, the compartment containing the CA functions as a secondary CA. The water protons on the outside of the compartment are affected by the overall magnetization of the magnetic bulk material inside that compartment, and are therefore relaxed by an outer-sphere mechanism. This long-range T_2/T_2^* relaxation effect is responsible for the blood oxygen level dependent (BOLD) effect, due to paramagnetic hemoglobin compartmentalized within blood erythrocytes, which is the basis of functional MRI (29). The effect depends on the magnetic moment and local concentration of the CA, the dimensions and geometry of the compartment, the diffusion constant of water, etc.

2.2.4. *Contrast effects*

At MRI fields, superparamagnetic agents have magnetic moments that are much larger (by a factor of 1000) than those of paramagnetic agents. Therefore, they have a much stronger long-range T_2/T_2^* effect than paramagnetic agents.

It can also be concluded that the classification of MR CAs as either 'T_1 agents' or 'T_2 agents' is not always accurate, since any CA that reduces T_1 also reduces T_2. However, any agent that reduces T_2 does not necessarily reduce T_1, at least at MRI field strengths. Whether the CA functions as a 'T_1 agent' or 'T_2 agent' depends on the imaging sequence used, the magnetic field strength, the size of the CA, and how the CA is compartmentalized in the tissue.

3. BIODISTRIBUTION AND APPLICATIONS

3.1. Introduction

In this section we will classify the CAs according to their biodistribution and the consequent applications of contrast-enhanced MRI techniques that they allow. Figure 1 describes a simplified scheme with the main distribution sites and excretion pathways for soluble metal complexes, such as the CAs, after being intravenously administered.

Among the CAs considered as *nonspecific agents*, i.e. those that do not interact specifically with any type of cells, one includes the *extracellular fluid (ECF) agents*, low molecular weight extracellular complexes that equilibrate rapidly between the intravascular and interstitial space and then are mainly excreted by the kidneys, and the high molecular weight *blood pool agents*, such as high generation dendrimers, which stay within the intravascular space and are slowly excreted via the kidneys and/or the liver. The *specific or targeted agents* can be considered in two groups: those that are passively directed to a particular type of cell, and those that are actively targeted to a molecularly specific site target with an appropriate ligand. The first group includes organ-specific agents for liver (*hepatobiliary*), spleen, lymph nodes, bone marrow or brain, mainly on the basis of agent size and chemical structure. The second group includes agents which target pathological processes or states, such as inflammation, atherosclerosis, angiogenesis, apoptosis and tumors. They are cell labeling CAs, as they work through recognition of specific molecular markers of those processes at the cell surface, such as cell-specific receptors or transport proteins, and accumulate at those molecular sites, usually in the intracellular space, and this can be used in molecular imaging applications of MRI. All CAs are organ-specific to some extent, as they are excreted either by the liver or the kidneys. There are also the *responsive, smart or bioactivated* agents, whose contrast is modulated by physiological parameters. Finally, one can consider organ-specific agents that are not injected, such as *oral agents*, which enhance the visualization of the gastro-intestinal (GI) tract, and *lung agents*, such as gases for lung imaging.

3.2. Extracellular fluid agents

After being intravenously injected, these agents leak rapidly from the blood pool into the interstitium with a distribution half-life ($t_{1/2}$) of about 5 min and are cleared mainly by the kidneys with an elimination $t_{1/2}$ of about 80 min (30–33). In areas with an intact blood–brain barrier (BBB), extravascular leakage of ECF agents into the brain will be prevented. Many brain pathologies,

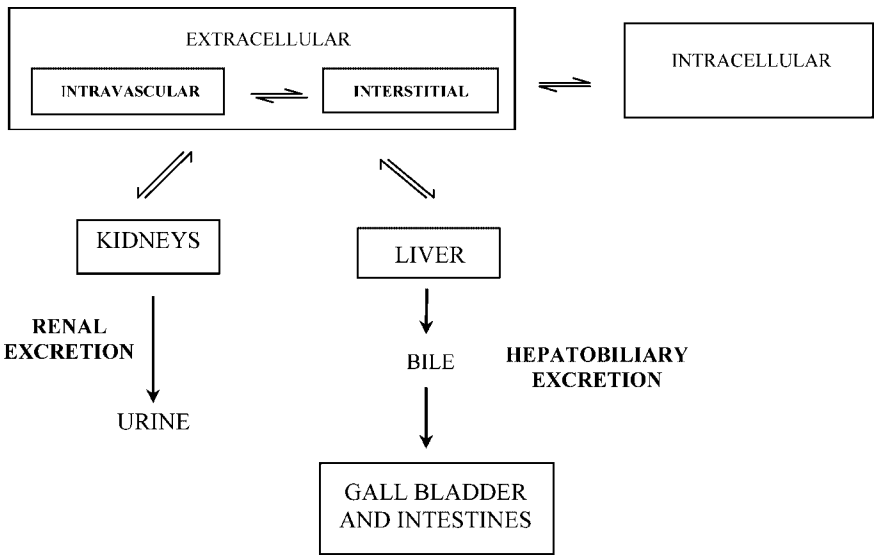

Figure 1. Main distribution sites and excretion pathways for intravenously administered soluble metal complexes.

however, are associated with an altered capillary permeability, which allows the selective accumulation of the administered CA in these regions and thus their better visualization by T_1-weighed MRI images. These ECF agents have also been extensively used in body imaging applications. They provide increased enhancement and visualization of lesions, such as tumors, e.g. in the spine and liver.

Some Gd^{3+}-based ECF agents have shown great utility in MR angiography (MRA). By selectively reducing the T_1 of blood water, their administration allows imaging of the vasculature and, thus, high-quality MR angiograms can be obtained. However, since these agents clear rapidly from the vasculature into the interstitial space, the MRA images are acquired in the so-called first-pass of the CA following a bolus injection. Given that the initial distribution half-life of the current ECF agents is short, there are several practical constraints: (a) the acquisition time window is very limited (usually to 1–3 min); in order to obtain the best possible vessel-to-background contrast, the MRA image acquisition has to coincide with peak arterial enhancement, otherwise significant artifacts occur, limiting the utility of the images obtained; (b) vessel-to-background contrast is limited because of the relatively low relaxivity of currently available ECF CAs; and (c) with the current generation of ultrafast MR imaging hardware, the vessel-to-background signal is reduced even further, for instance, when ultrashort *TR* values are used, especially for small diseased vessels.

ECF agents are typically Gd^{3+} chelates of linear or macrocyclic polyaminocarboxylate ligands, constituting the most important class of MRI CAs commercially available. They are divided into two groups, the *ionic* and the *neutral* agents (Fig. 2, Table 2). The ionic agents are meglumine salts of negatively charged chelates, which are hyperosmolar relative to blood. They include [Gd(DTPA)(H_2O)](NMG)$_2$ (gadopentetate bis-*N*-methylglucamine, Magnevist®, Bayer Schering Pharma AG), the first contrast agent to be approved for *in vivo* use in 1988, and [Gd(DOTA)(H_2O)](NMG) (gadoterate *N*-methylglucamine, Dotarem®, Guerbet). The neutral agents are Gd^{3+} complexes of DTPA and DOTA derivatives, including [Gd(DTPA-BMA)(H_2O)] (gadodiamide, Omniscan®, GE Healthcare), [Gd(HP-DO3A)(H_2O)] (Gadoteridol, Prohance®, Bracco Spa), [Gd(BT-DO3A)(H_2O)] (gadobutrol, Gadovist®, Bayer Schering Pharma AG) and [Gd(DTPA-BMEA)(H_2O)] (Gadoversetamide, OptiMARK®, Mallinckrodt). These CAs have the advantage of having no charge, and thus perturbing to a lower extent the osmolarity of blood. Their increased safety allows them, in particular Gadovist®, to be used in higher concentrations in MRA studies.

Gd^{3+}-based ECF agents are usually safe when used in clinically recommended doses, and adverse reactions and side effects, such as allergy, are very rare. Recently, however, there have been concerns linking the use of some of these CAs with nephrogenic systemic fibrosis (NSF) (34,35). Nevertheless, the number of reported NSF cases in the USA (about 130) is extremely small

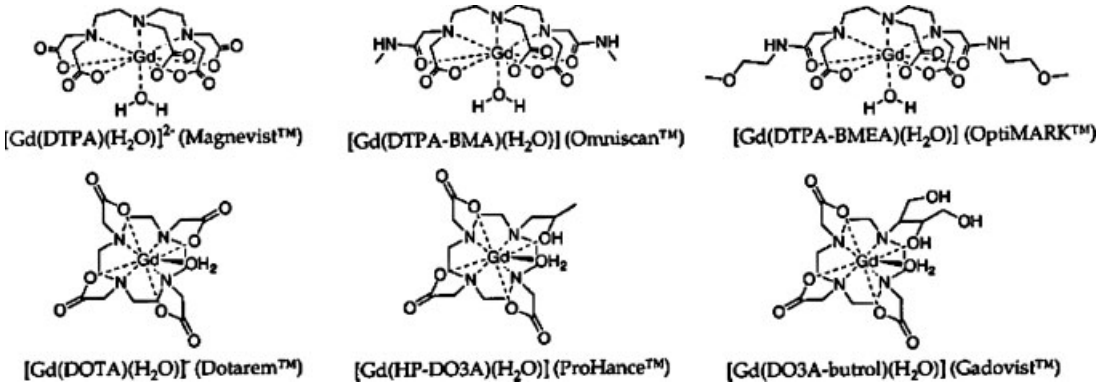

Figure 2. Structures of the commercially available ECF contrast agents (3).

Table 2. Properties of commercial ECF contrast agents with intravascular and extracellular distribution

Type	Name of compound	Central moiety	Relaxivity (1/mM/s) $B_0 = 1.0$ T (37°C)	Indication	Trade mark company
Ionic	Gadopentate dimeglumine, Gd-DTPA	Gd^{3+}	$r_1 = 3.4$, $r_2 = 3.8$	Neuro/whole body	Magnevist® Bayer Schering Pharma AG
	Gadoterate meglumine, Gd-DOTA	Gd^{3+}	$r_1 = 3.4$, $r_2 = 4.8$	Neuro/whole body	Dotarem® Guerbet
Neutral	Gadodiamide, Gd-DTPA-BMA	Gd^{3+}	$r_1 = 3.9$, $r_2 = 4.3$	Neuro/whole body	Omniscan® GE Healthcare
	Gadoteridol, Gd-HP-DO3A	Gd^{3+}	$r_1 = 3.7$, $r_2 = 4.8$	Neuro/whole body	Prohance® Bracco SpA
	Gadobutrol, Gd-BT-DO3A	Gd^{3+}	$r_1 = 3.6$	Neuro/whole body	Gadovist® Bayer Schering Pharma AG
	Gadoversetamide, Gd-DTPA-BMEA	Gd^{3+}	—	Neuro/whole body	OptiMARK® Mallinckrodt

Table 3. Different classes of blood pool agents currently in the market and under investigation

Type of blood pool agent	Description	Central moiety	Name of compound	Relaxivity (1/mM/s) (37°C)	Indication	Trade mark Company
Albumin binding molecules	Reversible or irreversible binding to albumin, macromolecular properties	Gd^{3+}	Diphenylcyclohexyl phosphodiester-Gd-DTPA, Gadofosveset (MS-325)	$r_1 = 19$, $B_0 = 1.5$ T	MRA vascularization, capillary permeability	Vasovist® Bayer Schering Pharma AG
		Gd^{3+}	B-22956 Gadocoletic acid	—	MRA	— Bracco SpA
		Gd^{3+}	Albumin-(Gd-DTPA)$_{30}$ Albumin-(Gd-DOTA)$_{30}$	$r_1 = 14.4$, $B_0 = 0.23$ T	MRA vascularization, MR-mammography	
		Dy^{3+}	Albumin-(Dy-DTPA)$_x$	T_2*enhanced	Blood flow perfusion	
Polymeric Gd complexes	Macromolecular properties	Gd^{3+}	(Gd-DTPA)-17 cascade polymer	$r_1 = 11.9$, $B_0 = 1.0$ T ($r_2 = 16.5$)	MRA vascularization	Gadomer-17 Bayer Schering Pharma AG
		Gd^{3+}	Gadomelitol, P-792	$r_1 = 42$, $B_0 = 0.47$ T ($r_2 = 50$)	MRA	Vistarem® Guerbet
		Gd^{3+}	(Gd-DTPA)$_n$-dextran		MRA	
		Gd^{3+}	Gd-DTPA-PEG polymers (polyethylene glycol)	$r_1 = 6.0$, $B_0 = 1.0$ T	MRA vascularization, capillary permeability	
		Gd^{3+}	MP 2269, 4-pentyl-bicyclo [2.2.2] octan-1-carboxyl-di-L-aspartyllysine-DTPA	$r_1 = 6.2$, $B_0 = 1.0$ T	MRA	
		Gd^{3+}	(Gd-DTPA)$_n$-polylysine	$r_1 = 13.1$, $B_0 = 0.23$T	MRA	Bayer Schering Pharma AG
Small Gd complexes	Susceptibility	Dy^{3+}	Dy-DTPA	T_2*enhanced	Blood flow perfusion	
		Dy^{3+}	Sprodyamide, Dy-DTPA-BMA	T_2*enhanced, $r_1 = 3.4$, $r_2 = 3.8$, $B_0 = 0.47$ T	Blood flow perfusion	
Mn-hydroxyapatite	Large particles	Mn^{2+}	Manganese substituted hydroxylapatite PEG-APD (MnHA/PEG-APD)	$r_1 = 21.7$, $r_2 = 26.9$, $B_0 = 1.0$ T	MRA	
USPIO particles	Coated iron oxide particles	Fe^{3+}/Fe^{2+}	ferumoxtran-10 AMI-227	$r_1 = 22.7$, $r_2 = 53.1$, $B_0 = 1.0$ T	MRA	Sinerem®, Guerbet; Combidex® AMAG Pharma
		Fe^{3+}/Fe^{2+}	SHU555C	$r_1 = 14$, $B_0 = 1.5$ T	MRA	Supravist™, Bayer Schering Pharma AG
		Fe^{3+}/Fe^{2+}	Fe O-BPA USPIO		MRA	
		Fe^{3+}/Fe^{2+}	MION, monocrystalline iron oxide nanoparticles	$r_1 = 3.7$, $r_2 = 6.5$, $B_0 = 0.47$T	MR-angiography, MR-lymphography tumor detection, infarction	

when compared with the millions of patients who have been exposed to the CAs, which makes the overall risk of developing NSF very low. The cases of NSF so far have been seen only in patients with severe kidney failure and there have been no reports of the problem among patients with normal kidney function or those with mild-to-moderate kidney insufficiency. NSF appears to be related to the release of Gd^{3+} by the kinetically less inert CAs, when they accumulate for a long time in the kidneys of those patients with severe kidney failure (36).

3.3. Blood pool agents

Blood pool agents (BPA) or intravascular agents are significantly larger in size than ECF agents and have higher r_1 relaxivities. Because of these characteristics, they offer many advantages in MRA relative to ECF agents. Their high molecular weight (>20 kDa) prevents leakage into the interstitium and they remain in the intravascular system for a prolonged time compared with conventional ECF agents. The long intravascular half-life and the high r_1 relaxivity allow imaging of the vasculature with higher vessel-to-background signal ratio (37). At the same time, their r_2 relaxivity must be low enough to avoid excessive signal loss due to T_2/T_2^* relaxation. By selectively reducing the T_1 of blood, high-quality angiograms can be obtained, including coronary artery imaging (38). The concentration of the CA in the plasma remains stable over one hour, as its mainly renal elimination requires the previous degradation of the macromolecule. This extends the imaging window from about 1 min to about 1 h. This advantage of BPAs over ECF agents of longer image acquisition times allows higher resolution and/or better signal-to-noise ratio and leads to better-quality angiograms of several organs using respiratory or cardiac gating techniques. Vascular abnormalities, associated with certain tumors or atherosclerosis, can be detected and MR mammography is feasible (39). Another advantage of using BPAs is that tissue blood volume and perfusion can be measured. Blood pool-enhanced MRA in the equilibrium phase (or steady state), as opposed to imaging during the initial arterial passage of the CA, offers the advantage of allowing the enhancement of both arteries and veins.

The blood pool CAs can be divided into several classes, according to their mechanism of action (Table 3): (a) the noncovalent binding of low molecular weight Gd^{3+}-based complexes to human serum albumin (HSA), which is the most abundant plasma protein (0.67 mM or 4.5% concentration in the blood plasma), prevents immediate leakage into the interstitial space; (b) systems based on polymers or liposomes, based on an increase in the size of the CA molecule, which slows down leakage through endothelial pores; and (c) systems based on particles, involving a change in the route of elimination. Other systems that are also being explored are small ECF Gd^{3+} complexes and Mn^{2+}-labeled hydroxyapatite particles.

3.3.1. *Albumin-binding gadolinium complexes*

This is the most successful approach so far. In this class, several complexes have been synthesized by attaching a hydrophobic moiety to a chelating agent, such as [Gd(DOTA-BOM_3)] (40). The most successful among these is the Gd^{3+} complex gadofosveset trisodium, previously known as MS-325 (Fig. 3), which became the first commercial agent in this class (Vasovist®, Bayer Schering Pharma AG). It binds strongly and reversibly to serum albumin (41), leading to high relaxivity at clinical field strengths and much longer residence times in the blood compared with extracellular agents (42). Several clinical studies have demonstrated its efficacy in enhancing blood vessels, both in first-pass and in delayed steady-state MRA examinations.

The second most valuable compound in this class is B-22956 or gadocoletic acid (Fig. 3; Bracco SpA). B-22956 is a Gd-DTPA derivative containing a cholic acid moiety with strong albumin binding (43). This again leads to much longer residence times in the blood and a higher relaxivity compared with the unbound form of the CA. B-22956 has been investigated for MR coronary artery imaging in clinical trials and to follow antiangiogenesis therapy (44), but is not yet commercially available.

The albumin-binding Gd^{3+} complexes have a wide range of applications besides MRA, e.g. breast MRI, perfusion MRI, lung perfusion, etc. Malignant tumors often show an increased uptake and metabolism of plasma proteins, especially albumin. Macromolecular CAs are delivered to all tissues, but only accumulate in those with leaky vessels near tumor capillaries (tumor neo-vessels). The outcome of tumor therapy can be followed using MRI tumor perfusion studies with Gd^{3+}-labeled albumin using the quantitative decrease in the MR signal of the malignant tissue after therapy.

3.3.2. *Polymeric gadolinium complexes*

The large size of polymeric Gd^{3+} chelates is responsible for the slow (or absent) leakage of this class of CAs into the interstitial space through the normal endothelium of the vascular system, thus providing long imaging windows. Various polymeric agents (e.g. dextrans and polylysine derivatives) with molecular weights in the 15–5000 kDa range were evaluated, but did not pass beyond the preclinical stage (45). Their large size leads to slow rotational dynamics and increased relaxivity at clinical field strengths. Excretion of Gd^{3+}-based macromolecular CAs is related to their size. Since the molecular weight of these large molecules exceeds 40 kDa, glomerular filtration decreases, which could lead to problems with their excretion, even if they are excellent MRA agents.

An example of this class of CAs undergoing clinical trials is Gadomer 17 (Bayer Schering Pharma AG), which carries 24 Gd^{3+} ions (46). Because of their size (molecular weight 35 kDa), Gadomer 17 molecules are large enough to show much slower leakage through normally functioning endothelium than extracellular agents, but are still small enough to be eliminated via the kidneys. Imaging studies in animals have resulted in excellent angiograms, allowing quantitative perfusion studies of the myocardium. It has been also successfully employed to demonstrate differences in endothelial permeability between tumors and healthy tissue (47).

$(Gd\text{-}DTPA)_{45}$-HSA is another example of this type of CA. Aime *et al.* (48) have studied the frequency and temperature dependence of proton and oxygen-17 relaxivities of this CA. The observed behavior is typical of systems whose relaxivity is limited by a long exchange lifetime of the coordinated water molecule (49). Sieving *et al.* (50) have synthesized a poly-(L-lysine) containing 60–90 chelating groups (DTPA or DOTA). Complexed with Gd ions, the paramagnetic chains were conjugated to HSA. The relatively small relaxation enhancement shown by Gd complexes when bound to polylysine is accounted for by the high internal mobility of the paramagnetic moiety. An analogous result has been observed using the squaric acid unit as a linker between the macromolecule and the Gd chelates (51). Labeling of monoclonal

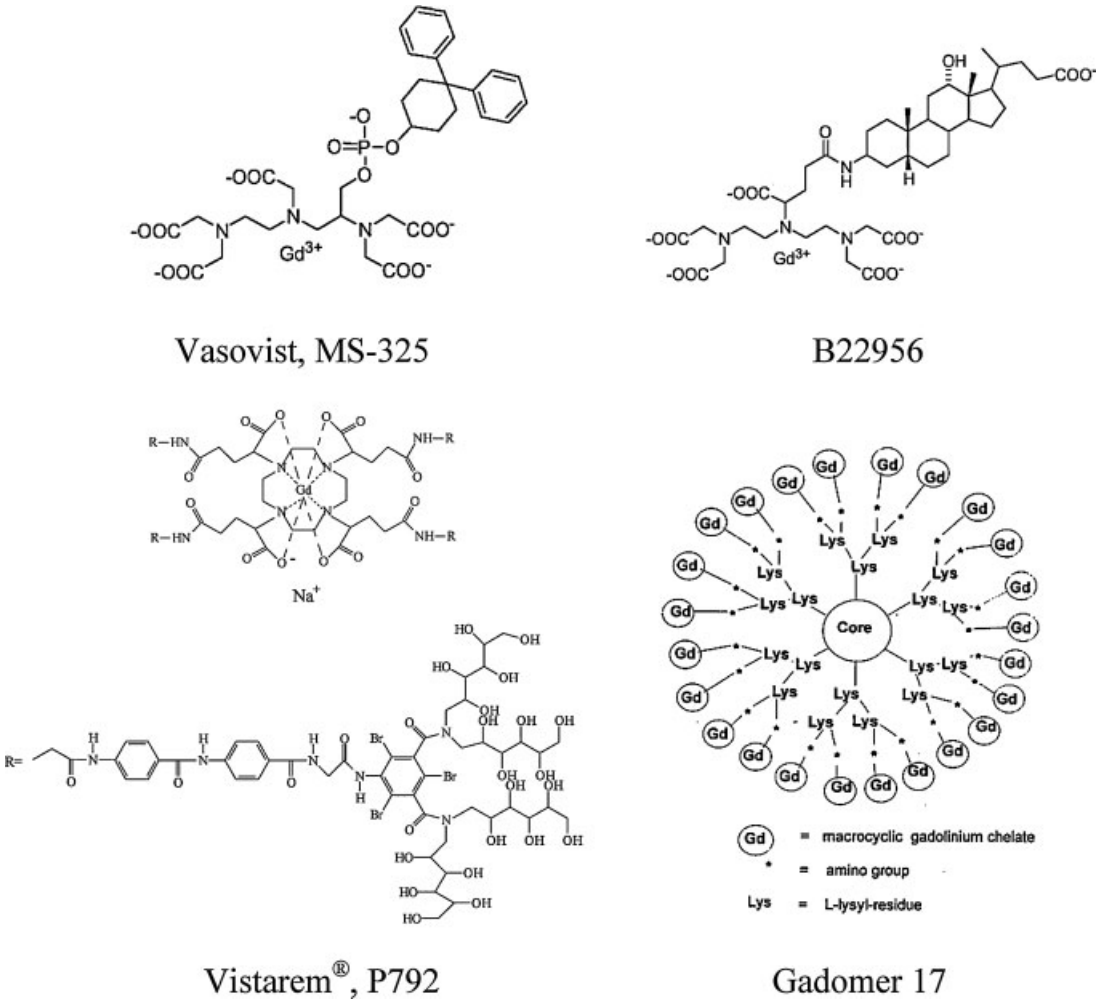

Figure 3. Structures of some HSA-binding and polymeric Gd^{3+} complexes, as potential or approved blood pool CAs for MRA (simplified structure for Gadomer 17) (9,46,55).

antibodies with Gd-DTPA has also been considered for targeting tumors (52,53).

The clinical application of Gd chelates grafted with polymers is limited by the slow excretion of the complexes and the resulting accumulation of toxic Gd^{3+}. To avoid this problem, biodegradable polydisulfide macromolecular complexes have been prepared based on the disulfide-thiol exchange in order to allow degradation of the macromolecules by endogenous thiol and thus facilitate excretion of the Gd chelates (54).

Another agent of this class undergoing clinical trials is P-792 (Gadomelitol, Vistarem®, Guerbet), a hydrophilic high molecular weight derivative of Gd-DOTA. This is a rapid clearance blood pool agent, owing to its limited diffusion across the normal endothelium, with high proton relaxivities r_1 and r_2 in the current range of clinical imaging magnetic fields (55).

The polymeric agent $(Gd\text{-}DTPA)_n$-polylysine, under development (PLLGd-DTPA, preclin., Bayer Schering Pharma AG), shows advantages in MRA, in perfusion studies of the myocardium and lung perfusion, and in the differential diagnosis of tumors. However, none of the polymeric Gd^{3+} complex CAs are yet commercially available.

The loading of micelles and liposomes with amphiphilic polychelate polymers has been reported also and different paramagnetic agents have been encapsulated into the liposomes (56). However, these studies did not lead to any agent which passed the preclinical status.

3.3.3. *Ultrasmall superparamagnetic iron oxides*

Superparamagnetic iron oxides (SPIOs) are nanoparticles made of stabilized iron oxides with very high T_1 and T_2 relaxivities (57). Similarly to the polymeric gadolinium chelates, these agents exhibit very slow leakage from the intravascular space due to their large size. At low doses they decrease the T_1 of blood and at higher doses the T_2^* effect predominates. Smaller-sized particles (USPIOs), such as ferumoxtran-10 (Sinerem®, Guerbet; Combidex®, ferumoxtran, Advanced Magnetics), SHU555C (Supravist™, Bayer Schering Pharma AG) and VSOP-C184 (Ferropharm GmbH), exhibit lower relaxivities than SPIOs, but have a much more favorable T_1/T_2^* ratio, which makes MRA and other T_1-weighted MR techniques even easier (22,58,59).

Unlike polymeric Gd^{3+} chelates, iron oxide agents are eliminated from the body by uptake into the liver, spleen and lymph nodes through the RES and subsequent incorporation into the body's iron pool. This takes much longer than simple excretion through the kidneys. USPIOs do not accumulate in the RES system as fast as larger particles, which results in a long plasma half-life (60). One of the agents in this class, Sinerem®,

Table 4. Hepatobiliary (liver) contrast agents

Type of agent	Name of compound	Central moiety	Relaxivity (1/mM/s) (37°C)	Distribution	Indication	Trade mark
Small complex	Gadoxetic acid, Gd-EOB-DTPA	Gd^{3+}	$r_1 = 5.3$, $r_2 = 6.1$, $B_0 = 0.47$ T	Hepatobiliary	Liver lesions	Primovist™ (formerly Eovist®) Bayer Schering Pharma AG
	Gadobenate di-meglumine, Gd-BOPTA	Gd^{3+}	$r_1 = 4.6$, $r_2 = 6.2$, $B_0 = 1.0$ T	Intravascular, extracellular, hepatobiliary	Neuro/whole body, liver lesions	Multihance® Bracco SpA
	Mangafodipir trisodium Mn-DPDP, Manganese dipyroxyl diphosphate	Mn^{2+}	$r_1 = 2.3$, $r_2 = 4.0$, $B_0 = 1.0$ T	Hepatobiliary, pancreatic, adrenal	Liver lesions	Teslascan® GE Healthcare
	Fe-HBED	Fe^{2+}		Hepatobiliary	Liver lesions	
	Fe-EHPD	Fe^{2+}		Hepatobiliary	Liver lesions	
	Chromium diethyl HIDA meglumine, Cr-HIDA	Cr^{3+}				
Paramagnetic liposomes	Liposomes, paramagnetic	Gd^{3+}		RES-directed	Liver lesions	
	Mn-EDTA-PP (liposomes)	Mn^{2+}	$r_1 = 37.4$, $r_2 = 53.2$, $B_0 = 0.5$ T			Memosomes
Particles	Ferrum oxid. (USAN), SPIO, AMI-25, dextran-coated	Fe^{2+}/Fe^{3+}	$r_1 = 40.0$, $r_2 = 160$, $B_0 = 0.47$ T	RES-directed	Liver lesions and control	Endorem™ Guerbet Feridex® AMAG Pharmaceuticals
	Ferrixan, Carboxy-dextran coated iron oxide nanoparticles, SHU 555A	Fe^{2+}	$r_1 = 25.4$, $r_2 = 151$ $B_0 = 0.47$ T	RES-directed	Liver lesions	Resovist ® Bayer Schering Pharma AG
	USPIO ferumoxtran-10 AMI-227	Fe^{3+}/Fe^{2+}	$r_1 = 23.3$, $r_2 = 48.9$, $B_0 = 0.47$ T	Vascular, lymph versus hepatocyte (AG-USPIO)	MRA vascular staging of RES-directed liver diseases	Sinerem®, Guerbet; Combidex® AMAG Pharmaceuticals
	Magnetic starch microspheres	Mn^{2+}/Mn^{3+}	$r_1 = 27.6$, $r_2 = 183.7$, $B_0 = 1.0$ T	RES-directed	Liver lesions, spleen	
	PION, polycrystalline iron oxide nanoparticles (larger particles = DDM 128, PION-ASF)	Fe^{2+}/Fe^{3+}	T_2*enhanced, $r_2/r_1 = 4.4$	RES-directed lymph versus hepatocyte	Liver lesions, MR lymphography	

cannot be administered by rapid bolus injection. Although it may be potentially useful for MRA, it is primarily developed for lymph node imaging (61).

3.4. Organ-specific agents

3.4.1. Hepatobiliary contrast agents

The diagnosis of hepatic lesions continues to be a problem even though many diagnostic methods are available. Despite the high contrast resolution of T_2-weighted MRI techniques, a number of pathologies are difficult to detect or differentiate without CAs. ECF agents (e.g. Magnevist®) rapidly distribute in the vascular and interstitial space, but do not pass plasma membranes and thus have negligible hepatocellular uptake and biliary excretion. Targeting the hepatocytes or entrapping substances in macrophages of the reticuloendothelial system (RES) are effective approaches for liver-specific agents since both pathways have a high capacity for handling relatively unspecific materials.

Several compounds with different magnetic properties are currently in clinical use, trials, or in preclinical development. The properties of some of them are shown in Table 4. They are divided in two main categories: (a) agents targeting *hepatocytes*—small paramagnetic complexes; and (b) agents targeting the *RES*—magnetic particles and magnetic liposomes.

Agents targeting hepatocytes: small paramagnetic chelates

The small water-soluble paramagnetic chelates with hepatobiliary uptake in clinical use (see ligand structures in Fig. 4) are the Gd-DTPA derivatives [Gd(EOB-DTPA)(H_2O)]Na_2 [gadoxetic acid disodium, Primovist™ (formerly Eovist®), Bayer Schering Pharma AG] and [Gd(BOPTA)(H_2O)](MEG)$_2$ (gadobenate dimeglumine, MultiHance®, Bracco SpA) and the Mn^{2+} chelate [Mn(DPDP)]HNa_3 (mangafodipir trisodium, Teslascan®, GE Healthcare).

The extracellular Gd-DTPA-type derivatives exhibit the most useful characteristics. Both have one lipophilic residue attached to the DTPA backbone that targets the agent to an organic anion transporter in the sinusoidal plasma membrane of the hepatocyte. The uptake by hepatocytes decreases T_1 and increases the signal intensity of normal liver parenchyma, giving a positive contrast relative to other tissues. These CAs display a very pronounced hydrophilic character and relatively low plasma protein binding, despite the presence of the lipophilic moiety, which gives them an acute intravenous tolerance as good as that of Magnevist®. $[Gd(EOB\text{-}DTPA)(H_2O)]^{2-}$, with the ethoxybenzyl group (62), is completely eliminated from the body, with 50% hepatobiliary and 50% renal excretion. After entering the intracellular space of the hepatocyte, it is sequestered in the bile. The excretion through the bile and feces causes the bile ducts and the gall bladder to display a very short T_1, which makes contrast-enhanced cholangiography possible. Shortly after administration, the compound distributes in the vascular system in the same way as Magnevist®, allowing the blood vessels to be seen in dynamic imaging studies. While the Gd^{3+} concentration and the signal intensity in blood decrease, the signal of the liver parenchyma increases, reaching maximum brightness 30–60 min after injection (63). $[Gd(BOPTA)(H_2O)]^{2-}$ has a benzyloxy lipophilic moiety bound to the DTPA backbone at a different position, providing similar properties to the above described chelate (64). In addition to the liver, it can be used for MRI of the brain and spine. Both Gd^{3+} agents significantly bind to HSA, although with affinities at least one order of magnitude lower that for the HSA-binding blood pool agents (65). Because of the resulting increased relaxivity and half-life in blood, they can be also used in MRA applications (66).

$[Mn(DPDP)]^{4-}$ (67) is the first Mn^{2+} complex to be used as contrast agent in clinical trials (68). The ion is a powerful T_1 relaxation agent because of its five unpaired electrons. This CA, which demonstrates both biliary and renal excretion, has been shown to be a positive and very effective liver enhancer in T_1-weighted images. Pharmacokinetic studies have shown that, shortly after injection, some Mn^{2+} is released in the plasma and the paramagnetic ion accumulates in the liver and other tissues like pancreas and cardiac muscle. Free Mn^{2+} ions are known to accumulate in hepatocytes, although the chemical similarity of

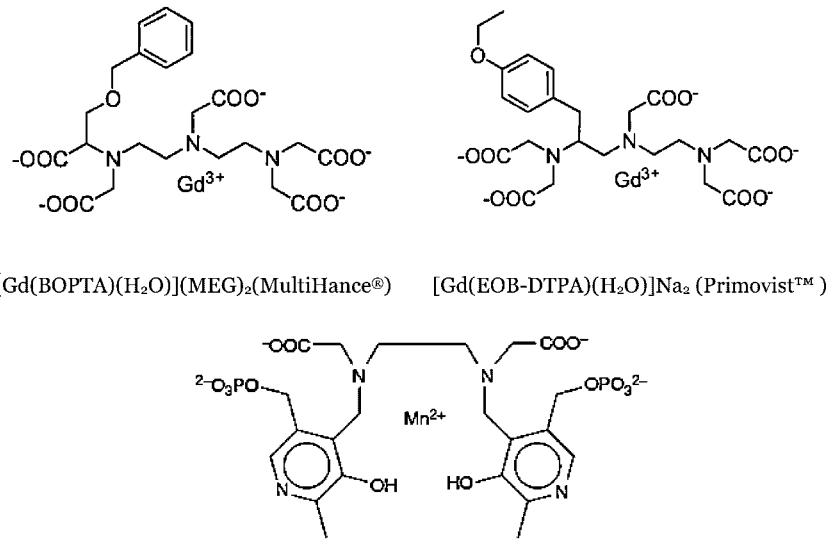

Figure 4. Chemical structures of the water-soluble paramagnetic chelates with hepatobiliary uptake in clinical use (9).

DPDP to vitamin B_6 may also contribute to hepatocyte uptake. Since Mn^{2+} is a powerful relaxation enhancer, a very small amount (5 μmol/kg) is sufficient to significantly enhance the contrast between the healthy liver parenchyma and focal liver lesions.

Other compounds have been investigated without clinical outcomes, such as Fe^{2+} chelates of EHPD or HBED, ligands similar to bilirubin, and Cr^{3+}-HIDA (Table 4).

Agents targeting the RES

Superparamagnetic iron oxide particles. These particles are extremely effective T_2 relaxation agents. After intravenous administration, SPIO particles are not retained in hepatocytes or metastases, but are sequestered by normal RES phagocytic Kupffer cells in liver and spleen, which represent a relatively small volume of the target (in the case of the liver only about 2–3% of its total cell population). However, their T_2 effect is so strong that even a very small dose is sufficient to decrease the signal intensity of the whole liver. This susceptibility effect is especially evident in T_2-weighted images in the form of a negative contrast. SPIOs are metabolized into a soluble and nonsuperparamagnetic form of iron, which is incorporated into the normal iron pool (e.g. ferritin, hemosiderin, hemoglobin) within a couple of days. Several preparations have been investigated, among which are two SPIO formulations that are now commercially available: AMI-25 (Feridex®, AMAG Pharmaceuticals, or Endorem™, Guerbet) and Resovist® (Bayer Schering Pharma AG) (Table 3) (69).

Paramagnetic liposomes. Paramagnetic liposomes are rapidly sequestered by the cells in the RES, primarily in the liver, giving positive (T_1-shortening) contrast. No compound of this kind has become commercially available.

There are two benefits of small chelates targeted to hepatocytes relative to SPIOs for Kupffer cells: (a) the higher number of hepatocytes than Kupffer cells improves the uptake effectiveness of the CA; and (b) their faster excretion reduces the possibility of side effects, compared with RES targeted CAs that remain longer in the body.

Hepatobiliary agents can be used to image liver pathologies. The small chelates can detect primary liver tumors or metastases (the majority of hepatocellular carcinomas), cysts and other benign lesions, which do not contain hepatocytes or whose functioning is hampered. SPIO-enhanced images during the retention phases offer improved diagnostic accuracy in detecting liver lesions. Since hepatic tumors either do not contain RES cells or their activity is reduced, the contrast between the liver and the lesion is improved as the lesion appears with positive contrast relative to the normal tissue. Resovist® does not accumulate in metastases, but some uptake is observed in hepatocellular carcinoma (HCC) and focal nodular hyperplasia (FNH). Feridex® is also not taken up by most tumors. Tissues such as metastases, primary liver cancer, cysts and various benign tumors, adenomas and hyperplasia retain their original signal intensity, so the contrast between normal and abnormal tissue is increased (70).

3.4.2. Contrast agents for lymph nodes and bone marrow

USPIOs do not accumulate in the RES system as fast as larger particles, which results in a long plasma half-life. USPIO particles, with a small diameter (less than 10 nm), are taken up from the interstitium by lymphatic vessels and transported to lymph nodes. Once within the nodal parenchyma, phagocytic cells of the mononuclear phagocyte system take up the particles. A lymph node with normal phagocytic function takes up a considerable amount of material and shows a reduction of the signal intensity caused by T_2 shortening effects and magnetic susceptibility. By comparison, metastatic lymph nodes take up a smaller amount of USPIOs so they appear with less signal reduction. This permits the differentiation of healthy lymph nodes from normal-sized, metastatic nodes. USPIOs also show potential for providing important information about angiogenesis in tumors and helping identify dangerous arteriosclerosis plaques. They can also accumulate in bone marrow.

Gadofluorine 8 (Bayer Schering Pharma AG) is a lipophilic but water-soluble gadolinium complex that accumulates in normal lymph nodes, resulting in a pronounced increase in their signal intensity, but not in malignant (metastatic) nodes, thus allowing their differential diagnosis (71).

3.4.3. Brain agents

Many brain pathologies are associated with an altered capillary permeability and disruption of the BBB, allowing the extravascular leakage of ECF agents into those brain regions, their selective accumulation and thus their better visualization by T_1-weighed MRI images. However, crossing an intact BBB is very difficult for a CA. An approach that has been used in animal models is microinjection of agents into selected brain areas. In the manganese-enhanced MRI (MEMRI) technique, the fact that Mn^{2+} can enter excitable cells via voltage gated calcium channels has been used to accumulate this ion in active areas of the brain and heart, leading to T_1 contrast (72). Direct injection of $MnCl_2$ into specific rat or mouse brain regions allows imaging of neuronal connections in their olfactory, visual and somatosensory pathways. Intraventricular microinjection of a low dose of potassium dichromate yields a specific contrast enhancement of white matter (WM) in T_1-weighted MRI images of mouse brain *in vivo*. Pronounced and persistent signal increases occur in other WM-rich brain areas, such as the corpus callosum, due to a tissue-specific reduction of diamagnetic Cr(VI) after injection forming paramagnetic Cr(V) and Cr(III), which relies predominantly on the oxidation of myelin lipids. Cr(VI)-induced contrast leads to only a small nonspecific enhancement of gray matter structures, such as the hippocampus. Thus, this method reveals novel information that differs from that obtainable using Mn^{2+} injection (73).

Noninvasive *in vivo* evaluation of amyloid in Alzheimer's disease (AD) patients would be useful for the early diagnosis of AD as well as the development and monitoring of new treatment strategies. Initial efforts to develop an MRI method to visualize the amyloid plaques were based on the assumption that the higher iron content in plaques would serve as an endogenous source of contrast that would be detectable at high fields through the susceptibility effect. Discrepancies observed in human post-mortem samples and the long, prohibitive, imaging time required for efficient *in vivo* visualization of the brain plaques showed the limitations of this approach. Then, transgenic mouse models of amyloidosis were used together with intravenous injection of Gd-DTPA tagged $A\beta_{1-40}$ peptides, covalently linked to putrescine (PUTGdAβ) to allow brain uptake. These peptides specifically target the amyloid deposits and thus improve sensitivity. They were also tested with an intracarotid co-injection with mannitol to permeabilize the BBB. This approach led to the first *in vivo* observation of AD plaques (74,75). The ability to label plaques efficiently after intravenous injection of the CA is a

Table 5. Oral contrast agents for imaging of the gastrointestinal bowel marking

Magnetism	Contrast	Name of compound	Central moiety	Relaxivity	Trade mark
Diamagnetic	Positive	Fatty emulsion	Fatty liquid	Short T_1	
		Vegetable oils	Fatty liquid	Short T_1	
		Sucrose polyesters	Fatty liquid	Short T_1	
	Negative	Perfluorooctylbromide (PFOB)	Water immiscible liquid	Proton density reduction, signal void	Perflubron®, Imagent GI® Alliance Pharmaceutical
		Barium sulfate suspensions and clay mineral particles	Ba^{2+}, Al^{3+}, Si^{4+}	Diamagnetic, T_2-short	Various mixtures
Paramagnetic	Positive	$MnCl_2$	Mn^{2+}	T_1 reduction	Lumenhance® ImaRx Pharmaceutical Corp. Bracco SpA
		[Gd(DTPA)]	Gd^{3+}	T_1 reduction	Magnevist enteral® Bayer Schering Pharma AG
		Ferric ammonium citrate Geritol	Fe^{3+}		Ferriseltz® Otsuka Pharmaceutical
		Gadolite 60 gastrointestinal, Gd-zeolyte Y particles	Gd^{3+}	T_1 reduction	Gadolite® Pharmacyclics
Superparamagnetic	Negative	Ferumoxsil (USAN) AMI-121	Fe^{3+}/Fe^{2+}	T_2^*enhanced	Lumirem® Guerbet Gastromark® AMAG Pharmaceuticals
		Ferristene (USAN) oral magnetic particles (OMP)	Fe^{2+}/Fe^{3+}	T_2^*enhanced	Abdoscan® GE Healthcare

significant improvement over existing MR plaque imaging methods. It also advances the possibility of monitoring experimental therapies aimed at clearing plaques in transgenic mice. Early plaque detection is not possible without the use of CAs, suggesting that these agents will be needed to diagnose Alzheimer's disease prior to the onset of clinical symptoms.

3.4.4. *Contrast agents for oral use*

When ingested, these agents change the signal intensity at the stomach and the intestine relative to adjacent abdominal tissues. They may change the contrast of the gastro-intestinal (GI) tract through various mechanisms, depending on their magnetic properties (Table 5), allowing MR cholangiography. *Diamagnetic* agents, such as fatty emulsions, fill the GI tract with materials with short T_1, enhancing its signal and producing positive contrast relative to adjacent tissues. Diamagnetic agents may also generate negative contrast either by decreasing the proton density through the use of perfluorinated compounds like perfluorooctylbromide (PFOB), or by decreasing the T_2 of GI water protons, such as in the presence of various mineral (Ba^{2+}, Al^{3+}, Si^{4+}) suspensions. *Paramagnetic* agents, such as $MnCl_2$ solutions, ferric ammonium citrate (FAC) solutions (76), Magnevist® or Gd^{3+}-containing zeolite Y particle suspensions (Gadolite®) (77), are positive CAs that decrease the T_1 of GI water protons. Large *superparamagnetic* particles for oral uptake (78), such as Abdoscan® (GE Healthcare), composed of monodisperse polymer particles of 3 μm diameter coated with crystals of iron oxide, or Lumirem® (Guerbet) (also known as GastroMARK® (AMAG Pharmaceuticals)), a silicone-coated superparamagnetic iron oxide suspension, belong to the group of negative oral CAs that decrease proton T_2/T_2^*. They are used to distinguish the loops of the bowel from other abdominal structures. When ingested, they flow through and darken the stomach and the small intestine in 30–45 min. By more clearly identifying the intestinal loops, they improve visualization of adjacent abdominal tissues such as the pancreas.

3.5. Active targeting or cell labeling contrast agents

These are targeted CAs that are able to recognize specific molecular sites (e.g. cell-specific receptors or transport proteins) at the cellular membrane and to accumulate at those sites, in most cases by becoming trapped in the intracellular space. The development of approaches able to recognize and image a specific molecular marker of a given pathological process or state (molecular imaging), such as inflammation, atherosclerosis, angiogenesis, apoptosis and tumors, makes the task of diagnosis and therapy much easier (79). Thus, the development of high affinity ligands as targeting vectors and their conjugation to Gd^{3+} chelates as reporter groups [Fig. 5(A)] is one of the requirements for efficient molecular probes.

However, the main problem of this approach using Gd^{3+}-based contrast agents is MRI's low sensitivity, so that to reach 50% of contrast enhancement it is necessary to have a local concentration of CA of the order of 0.5 mM. It is possible to increase the payload of reporter groups delivered at the target site by using many reporters bound to a single carrier [Fig. 5(B)].

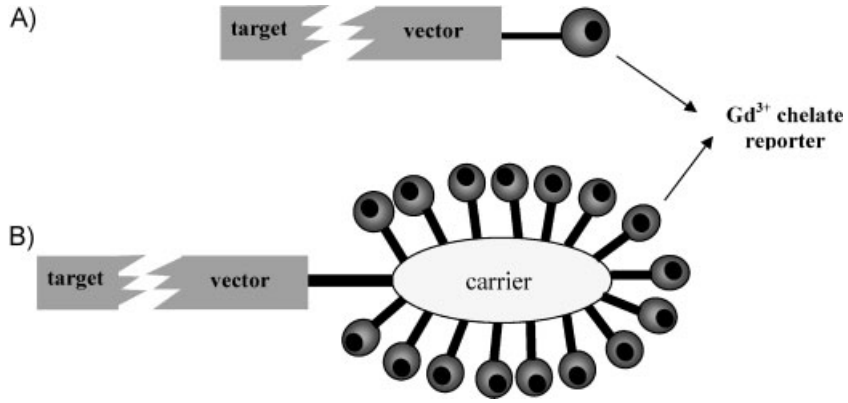

Figure 5. General structure of a targeted CA for cell labeling: (A) with a single reporter group; (B) with a carrier of many reporter groups.

However, this combined with the very low concentration of receptors in the cell membrane (10^{-9}–10^{-13} mol/g of tissue) makes it difficult to obtain an image with good contrast. Also, the saturation of all available receptors would interfere with the normal metabolic equilibrium, leading possibly to cell death (80). The minimum detectable concentration of a CA depends on its relaxivity. While for [Gd(HPDO3A)] ($r_1 = 3.7$/mM/s at 90 MHz) this value is too high (5×10^{-7} mol/g or 100 μM), for a sixth-generation dendrimer conjugate substituted with 170 Gd-DTPA chelates ($r_1 = 5800$/mM/s per dendrimer) it has a manageable value (1.9×10^{-10} mol/g). The use of SPIOs, with very high r_2 (72 000/mM/s per particle) further decreases this concentration to about 1.6×10^{-11} mol/g (81).

The main targeting strategies that have been used are cell surface targeting and receptor targeting. In the first approach, specific epitopes easily available at the cell surface are targeted to which the CA stays bound. This has been used together with the pretargeting approach to facilitate the detection and imaging of tumor cells (some of which are known to have abnormally high negative charges on their cell surface). This approach consists of a previous interaction of the tumor cell surface with a polypeptide formed by positively charged amino acids, such as polyarginine, that is suitable to interact with a negatively charged CA [Gd(DO3A)-R, where R = CH_2–C(=O) N(CH_2–PO_3^{2-})$_2$] that is added later (81). The use of low-molecular-weight targeting CAs, able to accumulate quickly at specific cell surface sites, has advantages relative to the use of macromolecular agents. One example is using targeting CAs based on the abnormal glycosilation of tumor cell surfaces, which have much higher content of sialic acid residues (>10^9/cell) than normal cells (~10^6/cell), where the sialic acid residues are recognized by a modified Gd^{3+} chelate (82).

Other relevant examples of cell surface targeting result from the well-known nonspecific binding of porphyrins to the interstitial space of tumors, e.g. Dy-TPPS (TPPS = tetraphenylporphyrin sulfonate). One expanded porphyrin (texaphyrin) complex, $[Gd(Tex)]^{2+}$ (PCI-120), selectively accumulates at tumor sites, giving prolonged enhancement of MRI images and the possibility of being used as a radiation sensitizer for brain cancer (83). Gadophyrin-2 [mesoporphyrin-$(GdDTPA)_2$] (Bayer Schering Pharma AG) targets the necrotic part of tumors, possibly through binding to cell proteins released upon cell death by necrosis. This specific accumulation of necrosis-avid CAs (NACAs) provides a prolonged enhancement of necrotic tissue, especially of myocardial infarcts (84).

The targeting of cell surface receptors can be pursued using labeled antibodies or low-molecular-weight targeting complexes. In the first approach, due to the slow diffusion of the antibodies, the most accessible targets are those present on the endothelial vessels. A typical example is the targeting of the endothelial integrin receptor $\alpha_V\beta_3$, a specific angiogenesis marker whose concentration correlates with the tumor grade. A Gd^{3+}-containing polymerized liposome was used as an example of an imaging probe containing many reporter groups per carrier. The pretargeting approach was used, where the target

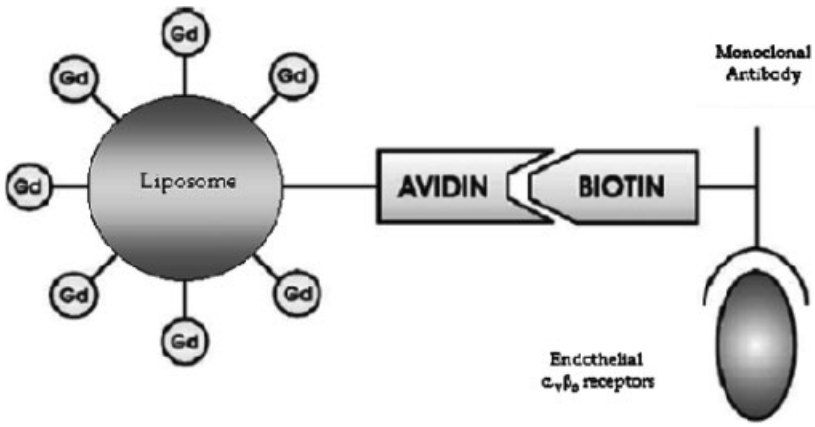

Figure 6. Schematic representation of targeting of the endothelial $\alpha_V\beta_3$ angiogenesis marker (85).

was bound first to a biotinylated monoclonal antibody against $\alpha_V\beta_3$, which is well recognized by an avidin moiety present on the liposome surface carrying the Gd^{3+} chelate reporter groups (Fig. 6) (85).

The same $\alpha_V\beta_3$ target has been addressed with lipidic nanoparticles containing Gd^{3+} chelates (86). Although the possibility of extensive substitution of some antibodies without loss of immunoreactivity has been demonstrated when they are labeled with liposomes, dendrimers or polymeric chelates, and nanoparticles, the large molecular size and, therefore, the slow delivery of these systems limit the technique.

A more efficient way to accumulate CAs at the target site is by cell internalization processes, which, to be successful, require that the concentration of the agent inside the cell is higher than at the cell surface. These internalization processes may occur via phagocytosis and pinocytosis (or fluid phase endocytosis) mechanisms, which do not require a cell receptor, or receptor-mediated endocytosis. Phagocytosis, the process of internalization of particles by cells endowed with phagocytic activity, has been used with Gd-DTPA bis-stearylamide derivatives forming insoluble Gd^{3+}-containing particles that, after internalization, are biodegraded and become soluble and trapped inside the cell (87). Gd-HPDO3A has been used for labeling stem cells via the pinocytosis mechanism, where the stem cells are incubated in a culture medium containing Gd-HPDO3A in the mM concentration range (10–50 mM) (88). However, these processes are often very slow and only apply efficiently to undifferentiated, dividing cells.

One example of cell internalization by receptor-mediated endocytosis is the entrapment of several units of a CA inside the inner spherical cavity of apoferritin, which after intravenous administration is quickly cleared up by specific receptors on hepatocytes (89). However, except in the case of internalization by electroporation, where it is delivered to the cytoplasm, the CA is entrapped in the cell endosomic compartment, seriously limiting its relaxivity (90).

Other cell internalization mechanisms have used membrane transporters and transmembrane carrier peptides. These latter have proven useful for the internalization of a number of substrates like proteins, oligonucleotides and plasmid DNA. For instance, translocating signal (MTS) peptides, such as the TAT peptide, made up of a sequence of 10 amino acids from the HIV-1 TAT protein, conjugated to iron oxide nanoparticles or to Gd-DTPA were efficiently internalized (91). Another interesting development was the synthesis of a bimodal (optical and MRI) imaging probe consisting of a Gd^{3+}/Eu^{3+}-DOTA complex, a PNA (peptide nucleic acid) sequence and a transmembrane carrier peptide. Although the system enters any type of cell, it accumulates only in tumor cells because of the specific binding of the PNA moiety to the c-myc mRNA whose production is upregulated in those cells. This bioshuttle conjugate—transporting the imaging probe into the cytoplasm and then into the nucleus—thus works as a nuclear localization sequence, and has proven to accumulate in the nucleus of DU-145 prostate cancer cells (92).

3.6. Responsive contrast agents

These agents are also called 'smart' or bioactivated. The term 'responsive' refers to paramagnetic systems that are sensitive to a given physico-chemical parameter that characterizes their microenvironment. Typical parameters to which these systems should be responsive are (a) pH, (b) temperature, (c) oxygen pressure, (d) enzymatic activity, (e) redox potential and (f) concentration of a specific ion. In the following paragraphs we will discuss some examples of reported studies of responsive CAs. We will differenciate between reports of properties of CAs studied in solution or in cells from those cases that have actually been used in a living animal or human by adding an asterisk next to each reference number if that publication contains data from an *in vivo* example. There are only a few of these applications *in vivo*. Quantitative information is hampered by the difficulty of knowing the local concentration of the agent.

3.7. pH-sensitive agents

These CAs are of great interest in cancer detection, as the pH on the surface of tumors is about 0.4 units lower than in normal tissue. The requirement for a system to be pH-sensitive is that either the dynamics or the structural properties determining its relaxivity are pH-dependent. The pH dependence of the relaxivity may reflect changes in the hydration number of the metal chelates, and the presence of protonatable groups on the ligands can influence these changes (93). In a tetraazamacrocyclic Gd^{3+} complex bearing an arylsulfonamide group as the pendant arm, it has been demonstrated that the observed decrease in the relaxivity with increasing pH in the pH 6–7 region is due to the change in the number of inner sphere water molecules in the complex from two at acid pH to zero at high pH (94). In another case, it has been demonstrated that the pH dependence of the relaxivity of GdDOTA-4AmP [amino phosphonate tetraamide derivative; Fig. 7(a)]. is due to changes in the second coordination sphere (95), which are related to the formation/disruption of hydrogen bonds between the pendant phosphonate groups and water molecules bound to the Gd^{3+} ion. This pH responsive agent was applied *in vivo* by assessing the local concentration of the CA through the use of the pH insensitive $Gd(DOTP)^{5-}$, assuming that the two have the same biodistribution. Extracellular pH MRI maps were thus obtained for mouse kidneys (96)* and rat gliomas (97)*.

Mikawa *et al.* (98) have developed an MRI contrast agent based on a microenvironmental responsive polyion complex in the form of a mixture of two polymers. The complex exhibits a 50% increase in relaxivity upon decreasing pH from 7 to 5. Aime and coworkers (99) have prepared a pH sensitive contrast agent with 30 Gd chelates and 114 ornithine residues [Fig. 7(b)]. The chelates are conjugated to the amino acid chain via squaric ester. At low pH, the amines are protonated and do not interact with the squaric esters linkers. When the pH rises, the amide side chains become deprotonated and interact with the squaric ester residues. This interaction rigidifies the polymer, causing an increase in τ_r and, thus, an increase in relaxivity. Lowe *et al.* (100) have synthesized a DO3A-derivative with a sulfonamide nitrogen that is protonated at low pH and unable to chelate the paramagnetic ion. As a result, water access to this ion is allowed, creating a detectable signal. At high pH the deprotonated amine chelates prevent water access and the MR signal is low. Hovland *et al.* (101) have prepared a DO3A compound with a tertiary amine-containing two long alkyl chains. When the amine is protonated (pH = 3–6) the relaxivity is low. Upon deprotonation (pH = 8–10), the agents form colloidal aggregates due to the higher lipophilicity. The aggregation causes an increase in τ_r and a subsequent increase in relaxivity. A Gd-DOTA-tetraamide bearing a hydroxypyridyl substituent has exhibited two regions of enhanced relaxivity: a small enhancement at lower pH = 2–4 attributed to an increase in the prototropic exchange of the

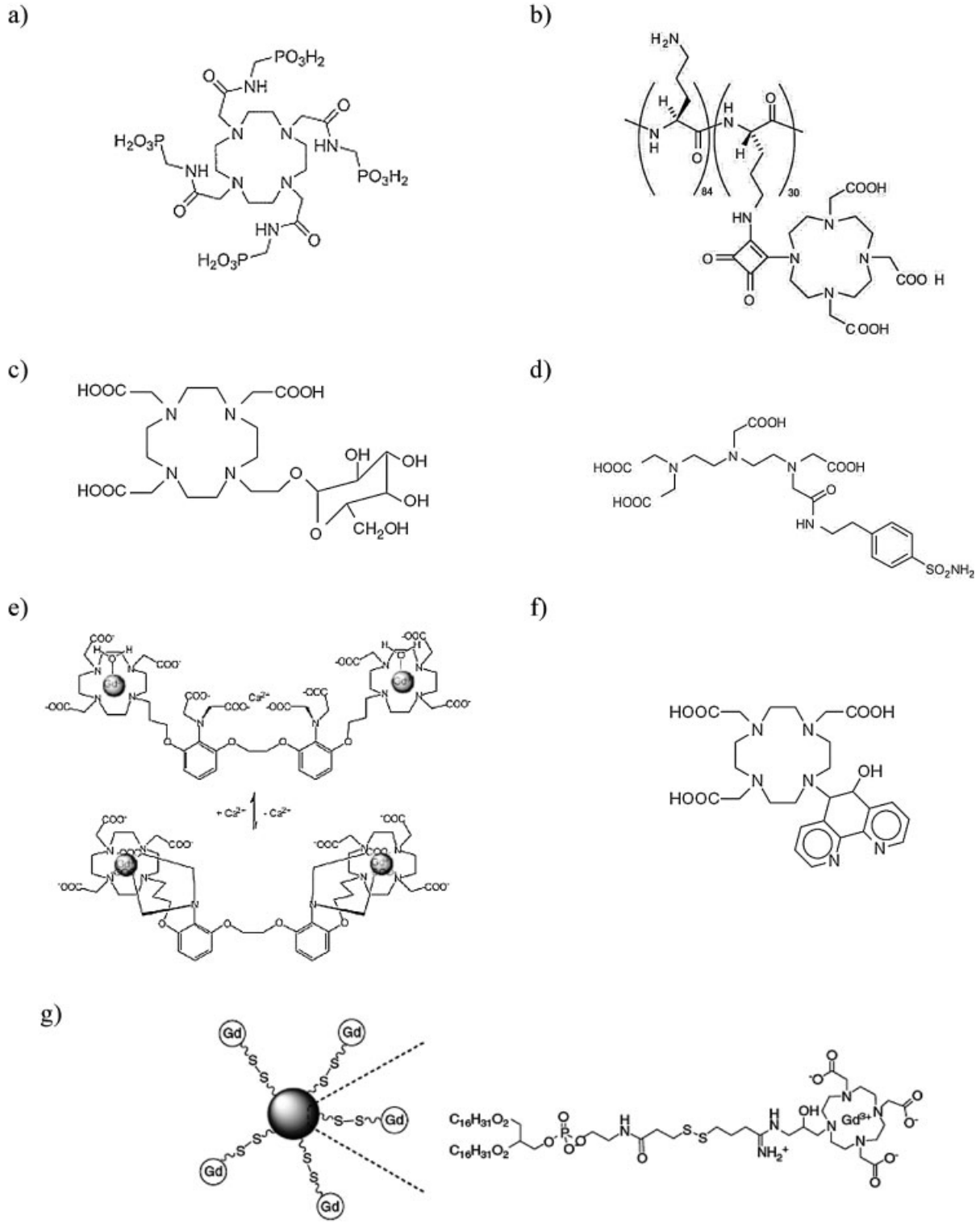

Figure 7. Chemical structures of some Gd^{3+} chelates as (or ligands present in) responsive CAs: (a) DOTA-4AmP; (b) macromolecular polyornithine DO3A; (c) DO3A-β-gal; (d) sulfonamide-substituted DTPA; (e) Gd_2(DOPTA) binding Ca^{2+}; (f) phenHDO3A; (g) Gd(HASH-DO3A) conjugated to DPPE PDP in liposome.

coordinated water molecule and a slightly larger enhancement at higher pH = 6–9 due to deprotonation of the ligand amide protons (102). Aime *et al.* (103) have also synthesized a ternary complex between a Gd chelate and carbonate ions. The relaxivity of this complex can be affected by the saturation of its coordination sphere by two water molecules or a bidentate ligand such as hydrogen carbonate. The relaxivity of the complex changes from 7.5/mM/s at low pH to 1.9/mM/s at high pH,

reflecting the replacement of two water molecules in the first coordination sphere by a carbonate ion. A water-soluble Gd^{3+}-fullerene has been reported in which the relaxivity is pH-dependent due to changes of self-association (104).

3.7.1. *Temperature sensitive agents*

It is known that some Ln^{3+} chelates have NMR properties which are strongly temperature dependent, such as their ^1H NMR chemical shifts, which can be used for monitoring temperature. For this reason, some of them are considered to be good temperature probes (105,106). Another example of a temperature-dependent probe consists of the encapsulation of Gd^{3+} chelates into liposomes (107). Here, the membrane transition from gel to liquid crystal occurs at a certain temperature. At this point, changes in the permeability of the membrane occur and the mobility of the water molecules through the membrane changes; consequently the relaxivity also changes.

3.7.2. *Agents sensitive to the redox potential*

The partial oxygen pressure (pO_2) is also an important parameter in the metabolic processes of the cells and its variation is related with certain pathologies. The systems used as pO_2 probes are based on the spin state or redox equilibria of paramagnetic ions. The use of deoxyhemoglobin as MRI contrast agent was discovered by Thulborn *et al*. (109)*, based on the pO_2 dependent high-spin/low-spin equilibrium of Fe^{2+}. Ogawa *et al*. (109)* have shown that the signal is dependent on the oxygenated state of blood and that the blood oxygen level-dependent (BOLD) signal can be used for the noninvasive mapping of human brain function. Activatable contrast agents, with relaxivities that depend on the oxidation state of the metal ion and thus on pO_2, have been synthesized (110). The oxidation state of a europium ion is varied to trigger the signal on and off by the environmental pO_2. Eu^{3+} is reduced to Eu^{2+} (isoelectronic with Gd^{3+}) and enhances the observed MR signal upon reduction. Aime *et al*. (111) have developed a redox switch to increase τ_r as a pO_2-sensitive compound. This complex uses manganese (Mn^{2+}) as the redox ion. By coupling the product to polycyclodextrin, the Mn^{2+} porphyrin aggregates, increasing the Mn^{2+} concentration and τ_r, the rotational correlation time. The water relaxation of Mn^{2+} is much greater than that of Mn^{3+}, creating a redox switch dependent on pO_2. This technique can quantify the oxygen concentration in the surrounding environment.

3.7.3. *Agents sensitive to enzyme activity*

The first enzymatic sensitive contrast agent was developed in response to the need to correlate biological events with gene expression during an imaging experiment. The mechanism is based on two distinct relaxation states, a weak and a strong one. The DOTA-type macrocyclic agent 'Egad' [Gd-(DO3A-β-gal); Fig. 7(c)] has a sugar moiety (a substrate of the enzyme β-galactosidase), which by blocking the single open coordination site excludes the water protons from the inner sphere so that the effect of the Gd^{3+} ions on the relaxivity is diminished. This agent is irreversibly activated when β-galactosidase cleaves the sugar and water becomes accessible to the paramagnetic ion, thus increasing the q number. This agent has been successfully used *in vivo* to detect by MRI β-galactosidase mRNA expression in living *Xenopus laevis* embryos (112)*.

Another approach is to use insoluble Gd^{3+} chelates, such as GdDTPA-FA, containing on the ligand surface two long fatty acid chains ($COOC_{17}H_{35}$) connected via an ester bond, which form inactive particles. The particles are internalized into dendritic cells by phagocytosis and solubilized by intracellular lipase activity through cleavage of the ester bonds to the insolubilizing moiety. Thus, the increase in intracellular r_1 relaxivity is a function of the activity of the enzyme. MRI images of the labeled cells implanted into rat brain have proven that these particles can act as positive T_1 agents and are suitable for functional cellular *in vivo* MRI. (113)*

Another example of an enzyme responsive agent is a linear Gd^{3+} complex possessing an arylsulfonamide moiety [Fig. 7(d)] that is an inhibitor of carbonic anhydrase (114). Here, the relaxivity of the agent is enhanced as a result of the increased reorientational correlation time τ_r upon interaction with the enzyme.

Nivorozhkin *et al*. (115) have prepared an agent that is sensitive to the presence of human carboxypeptidase B, which has been implicated in thrombotic disease. TAFI cleaves a trilysine masking group attached to the agent, exposing an aromatic functional group that has a high affinity for human serum albumin. The contrast agent binds HSA leading to an increase in τ_r. This event is known as a receptor-induced magnetization enhancement (RIME). The trilysine chain makes this agent a pro-RIME agent because the trilysine chain inhibits interaction with HSA.

Bogdanov *et al*. (116) have prepared a peroxidase activatable agent. This agent consists of a Gd^{3+} chelate linked to benzene-1,2-diol that acts as a monomer. In the presence of peroxide, the monomers are oligomerized, yielding a threefold increase in relaxivity due to an increase in τ_r. This MRI signal amplification can detect peroxidase concentration *in vitro* and has been used to detect E-selectin expression on human endothelial cells in culture by the high local enzymatic activity of antibody bound peroxidase associated with the plasma membrane of these cells.

Duimstra *et al*. (117) have synthesized a new class of enzyme activated contrast agents using a self immolative mechanism for detection of β-glucuronidase. Querol *et al*. (118) have prepared new DTPA bisamides as sensors of peroxidase activity. These derivatives bear tryptamido or 5-hydroxytryptamido groups that could be oligomerized *in situ* in the presence of a peroxidase–H_2O_2 pair resulting in a net increase in r_1 relaxivity. Chen *et al*. (119) have shown that activatable paramagnetic imaging agents can be used to directly image myeloperoxidase (MPO). Plaque rupture in atherosclerotic disease is the major cause of morbidity and correlates well with MPO secretion by activated macrophages and neutrophils in humans. Gd-DOTA-serotonin [3-(2-aminoethyl)-5-hydroxyindole] was efficiently polymerized in the presence of human neutrophil MPO resulting in a 70–100% increase in proton relaxivity.

3.7.4. *Metal ion and radical responsive agents*

The presence of metal ions can induce changes in the structure of the paramagnetic complexes, consequently changing their relaxivities. Intracellular calcium plays an important role in muscular contraction, neuronal transduction, and hormonal secretion. Li *et al*. (120,121) have developed a contrast agent, Gd_2(DOPTA) [Fig. 7(e)], that can specifically detect Ca^{2+} ions. In the absence of Ca^{2+}, the aromatic aminoacetates interact with the two Gd ions; but in the presence of Ca^{2+}, they rearrange to bind Ca^{2+}, allowing water to bind directly to Gd^{3+}. This increase

in q number yields an increase in relaxivity. This mechanism is reversible.

Hanaoka *et al.* (122,123) have used a similar scheme for the detection of zinc ions, with a ligand of DTPA with *N,N,N′,N′*-tetrakis (2-pyridylmethyl)ethylenediamine (TREN) as a zinc specific chelator. In the absence of zinc, water is bound to the gadolinium ion. In the presence of zinc, the carboxylic acid and pyridine moieties coordinate to zinc thus restricting the access of water to the Gd ion. This decrease in q yields a decrease in relaxivity in the presence of zinc.

An iron-sensitive contrast agent has been synthesized by Aime *et al.* (124) by functionalizing DTPA with salicylate moieties. Upon addition of iron (III), the Gd-DTPA–salicylate complexes bind to the iron ions via the salicylate functional groups. This binding yields an increase in τ_r and in relaxivity.

Another iron-sensitive contrast agent has been prepared by Comblin and Jacques (6,125). DOTA was conjugated to a phenanthroline derivative, giving PhenHDO3A [Fig. 7(f)], which is a ditopic ligand featuring a tetraazacyclododecane unit substituted by three acetate arms and one 6-hydroxy-5, 6-dihydro-1,10-phenanthroline group. This ligand was especially designed to obtain highly stable heteropolymetallic assemblies (126). Self-assembly around iron (II) ions leads to an increase in τ_r and a relaxivity increase from 3.7/mM/s, obtained for [Gd(PhenHDO3A)], to 12.5/mM/s for $\{Fe[Gd(PhenHDO3A)_3]\}^{2+}$ at 20 MHz and 37°C. Costa *et al.* (127) have developed the same kind of rigid chelates obtained by self-assembly of Fe(II) ions and two terpyridine-based Gd-DTTA. $\{Fe[Gd_2bpy(DTTA)_2(H_2O)_4]_3\}^{4-}$ is a self-assembled, metallostar-structured potential MRI contrast agent, with six efficiently relaxing Gd^{3+} centers confined into a small molecular space. Its proton relaxivity is particularly remarkable at very high magnetic fields ($r_1 = 15.8$/mM/s at 200 MHz, 37°C, in H_2O) (128)*. Recently, another high-molecular weight tetrametallic supramolecular complex $[(Ln\text{-}DTPA\text{-}phen)_3Fe]^{-}$ (Ln = Gd, Eu, La) has been obtained upon self-assembly around one iron(II) ion of three 1,10-phenantroline- based molecules substituted in 5′-position with the polyaminocarboxylate diethylenetriamine-*N,N,N′*, *N′,N′*-pentaacetate, DTPA- $phen^{4-}$ (129)*.

A radical responsive CA has been reported, which consists of Gd^{3+} chelates containing a free thiol group (Gd-HASH-DO3A) conjugated through a disulfide bond formed with SH-activated phospholipid molecules incorporated in a liposome [Fig. 7(g)]. The long reorientational motion of the supramolecular adduct endows the CA with an r_1 relaxivity significantly higher than that of the free complex. The disulfide bonds represent a radical-sensitive moiety and a large decrease in the relaxivity is observed upon their cleavage (130).

4. CONTRAST AGENTS BASED ON OTHER PROPERTIES

In addition to the CAs classified according to their biodistribution and the response of their relaxivity to physiologically relevant physical parameters, new classes of MRI CAs have recently been developed based on their NMR properties. Here we describe two such families.

4.1. Chemical exchange saturation transfer agents

A new class of CAs, chemical exchange saturation transfer (CEST) agents, has been shown to be a promising alternative to relaxivity-based CAs (131). A CEST agent is a molecule possessing exchangeable protons (-NH, -OH, etc.) that resonate at a chemical shift that is different from the bulk water signal, which happens when their exchange with the bulk water protons is slow on the NMR timescale. This occurs when $\Delta\omega \geq k_{ex}$, where k_{ex} is the exchange rate of the process and $\Delta\omega$ is the difference in frequency between the chemical environments. When this condition is fulfilled, radio frequency pulses applied at an appropriate frequency and power level can saturate the exchangeable protons of the CEST agent. These protons will then transfer into the bulk water pool and lead to a reduction of its equilibrium magnetization, with a resulting decrease of its signal intensity. Therefore, this water saturation process is caused by chemical exchange. CEST agents can be used to switch the image contrast 'on' and 'off' by changing the irradiation parameters.

Although several agents contain exchangeable protons and can produce CEST contrast (132), their signals are often very close to the bulk water signal, and often broader than 2 ppm, due to the magnetic field inhomogeneity of many tissues (133). This makes it difficult to distinguish contrast due to the CEST effect vs. direct saturation of bulk water. A larger $\Delta\omega$ value improves the specificity and efficacy of the CEST effect. Since $\Delta\omega$ increases with the magnetic field strength, it can be improved at higher field strengths for the MR experiment. Another possibility is to use paramagnetic complexes, displaying large $\Delta\omega$ values for the exchanging proton resonance. These paramagnetic CEST (PARACEST) agents include particular Ln^{3+} complexes with a coordinated water molecule undergoing extremely slow exchange with the bulk water, and with very large $\Delta\omega$ values. A good saturation transfer (ST) effect has been reported by irradiating the metal-bound water protons of Eu^{3+} chelates resonating at 50 ppm downfield from the bulk water (134). The same effect can be obtained with slow exchanging amide protons of Ln^{3+} complexes, e.g. tetraamide DOTA derivatives (135).

An advantage of CEST agents relative to the traditional MRI CAs is that the generation of contrast occurs only if the RF irradiation frequency is set equal to the absorption frequency of the mobile protons. For this reason, the acquisition of a precontrast image is not required because the image visualization of CEST agents results from the comparison of the on and off resonance MRI scan. Furthermore, a co-administration of different CEST agents at the same time is possible (since the difference on resonance frequencies of their mobile protons is large enough to avoid the overlapping of the respective CEST resonances), making it possible to detect their biodistribution in the same image (136). In this way, by using ratiometric methods, the CEST response can be made independent of the absolute concentration of the agent.

Responsive PARACEST MRI CAs have also been developed. Paramagnetic Ln^{3+} complexes of tetraamide derivatives of DOTA show ST properties which are markedly dependent on pH (137–139). This is because the amide proton chemical exchange is catalyzed by hydroxyde ions. Other PARACEST agents change their chemical exchange rates after binding to lactate (140), polyarginine (141), glucose (142), Zn^{2+} (143), etc., and detect temperature changes (144) or enzyme activity (145). These responsive agents share the same advantages and disadvantages with responsive relaxivity-based CAs (146).

The most critical disadvantage of (PARA)CEST agents is their low sensitivity. Theoretically, the ST process is dependent on a

number of parameters, among which k_{ex} and the number of mobile protons available are particularly relevant. Small-sized CEST agents, containing less than 10 mobile protons per molecule, such as amino acids, heterocyclic compounds, sugars or paramagnetic chelates, have the detection limit in the mM range (131,137,138,147). To solve this problem, some approaches have been suggested in order to increase the number of mobile protons in the CEST agents, such as the investigation of the ST properties in macromolecules, both diamagnetic (polyaminoacids, dendrimers and RNA-like polymers) and paramagnetic ones (147–149), sometimes exploring supramolecular interactions (SUPRACEST) (149), with which their detection limit goes down into the range of μM.

Another approach to improve the sensitivity of CEST agents is represented by liposomes, where the number of mobile protons which can be entrapped in their aqueous cavity is in the range of 10^6–10^9, depending on the liposome's size. Besides the water molecules, an efficient paramagnetic shift reagent, such as $[Tm(DOTMA)]^-$, can also be entrapped in the liposome cavity, shifting the proton resonance of trapped water relative to the bulk water. Because of the slow water exchange across the liposome membrane, this type of assembly, named LIPOCEST agent, can be used at nM concentrations to generate a CEST image (150).

Such a high sensitivity can be used to design targeted PARACEST CAs for molecular imaging applications. A fibrin targeted CA has been obtained by incorporating a phospholipid-conjugated Eu-DOTA derivative into the lipid layer of perfluorocarbon nanoparticles, which were targeted to clots by antifibrin antibodies. A contrast-to-noise ratio of 10 was produced at the clot surface in MRI images of plasma clots (151).

4.2. Hyperpolarized agents and molecular imaging using MRI

MRI provides unsurpassed soft tissue contrast, but its inherent low sensitivity has limited the clinical use to imaging of water protons. This is because the NMR signal is proportional to the thermal equilibrium polarization (population difference) of nuclear spins, which depends on the magnetic field strength and temperature, but is normally very low, for instance, 5×10^{-6} for ^1H and 1×10^{-6} for ^{13}C at 1.5 T and at body temperature. Some sensitivity improvement has been achieved using MRI systems at field strengths of 3–11.7 T, as the thermal equilibrium polarization increases with the magnetic field strength.

A totally different approach for increasing the polarization of spins is to create an artificial, nonequilibrium distribution of nuclear spins called the hyperpolarized state (152). In this state, the polarization of spins can be increased by a factor of $\sim 10^5$ compared with that in the thermal equilibrium state. This extraordinary gain in polarization translates directly into a gain in signal strength for MRI. The strong signal enhancement enables imaging of nuclei other than protons, e.g. ^3He, ^{129}Xe, ^{13}C, ^{15}N, ^6Li, and their molecular distribution *in vivo* can be visualized in a clinically relevant time window (153).

The nuclear spin polarization of the noble gas isotopes ^3He and ^{129}Xe can be increased by four to five orders of magnitude using optical pumping, a process in which light is used to raise (or 'pump') the nuclear spins of the gas molecules from a lower energy level to a higher one, so as to achieve the population inversion characteristic of the hyperpolarized (HP) state. This new technology of hyperpolarized gas MRI holds enormous potential for enhancing sensitivity and contrast in pulmonary imaging. Its applications range from MR microscopy of airspaces to imaging pulmonary function in patients (154). Li^+ is the major drug administered to patients with manic depression. Because of the low sensitivity of $^6Li^+$, with a T_1 of the order of several minutes, its use to study the distribution of lithium in the human brain by conventional MRI is not feasible. However, MRI detection and imaging of hyperpolarized $^6Li^+$ in the rat brain *in vivo* has been reported. The long T_1 of $^6Li^+$ is considerably shortened by Gd-DOTP, with a relaxivity of 11/mM/s, suggesting that the presence of 0.1–10 μM CAs should be detectable, provided sufficient sensitivity is available, such as that afforded by hyperpolarization (155).

A wide range of organic substances containing ^{13}C has been hyperpolarized by either parahydrogen-induced polarization (PHIP) (156) or by dynamic nuclear polarization (DNP) (157). The potential applications of hyperpolarized ^{13}C imaging include vascular imaging, perfusion imaging (158), catheter tracking (159), and visualization and metabolic/molecular imaging (152). The PHIP method increases the nuclear polarization by a chemical reaction of parahydrogen with a substrate containing double or triple bonds (160). In parahydrogen, the two hydrogen nuclei are oriented antiparallel. This is a nonequilibrium state in which the magnetic moments of the hydrogen nuclei cancel mutually (152).

In practice, the parahydrogen molecule is added as a whole unit onto substrates by rhodium-catalyzed hydrogenation. Then the nonequilibrium spin polarization of parahydrogen is converted to the nuclear polarization of a vicinal ^{13}C nucleus by diabatic–adiabatic magnetic field cycling or by radiofrequency (RF) pulses. Currently, polarization levels of 20–30% can be obtained by the PHIP method for a substrate such as 2-hydroxyethylacrylate (152). Its hydrogenated product, hyperpolarized (2-hydroxyethyl-propionate, abbreviated as HP[^{13}C]HEPP), can be injected into subjects at a concentration range of 0.3–1.2 M in 2–3 ml. The injected HP[^{13}C]HEPP can reach hearts and lungs in < 10 s in mice, at 2–40 mM concentration. This provides a reasonable time window to obtain signals in organs and detect changes in molecular structures associated with metabolic processes.

The magnetization of hyperpolarized ^{13}C is created outside the MRI imager in a polarized system. After hyperpolarization, the polarization return to the thermal equilibrium level occurs at a rate governed by T_1, which ranges from a few seconds to several minutes for ^{13}C, depending on the functional groups present. Hyperpolarized ^{13}C MRI, like positron emission tomography (PET) and single-photon emission tomography (SPECT), generates a signal with an amplitude that is directly proportional to the concentration of the imaging agent (161). However, PET and SPECT have much higher sensitivities, allowing for detection of tracers at 10^{-8} M. The lack of background signal is an advantage in angiography and perfusion. The small molecular size of HP[^{13}C]HEPP makes it an extracellular fluid (ECF) MRI CA. It remains mainly within the vasculature during the first few circulations in the body, then is distributed into the extracellular space, and is finally excreted through the kidneys (162).

The study of lung perfusion in normal and diseased subjects is of great interest to physiologists and physicians. Liquid-phase hyperpolarized (HP) ^{13}C tracers are very useful in MRI of the pulmonary vasculature and pulmonary perfusion, because of the high spatial and temporal resolution of the images that are obtained with this contrast technique, which overcomes the insufficient signal of classical MRI for quantitative functional assessments (162).

^{13}C-labeled endogenous compounds that can be hyperpolarized by the DNP technique have significantly extended the applications of metabolic imaging, e.g. in tumor diagnosis. The metabolic fate of C_1-^{13}C-pyruvate in images of tumor-bearing animals injected with hyperpolarized labeled pyruvate has been followed using the DNP-MR technique, and allowed mapping the metabolic pattern of labeled pyruvate, as well as of lactate and alanine. It was confirmed that the hyperglycolic cancer cells abundantly transform pyruvate into lactate and alanine through anaerobic glycolysis (163). Cardiac metabolic imaging with hyperpolarized C_1-^{13}C-pyruvate has been recently shown to be feasible (164). C_1-^{13}C-pyruvate is part of the energy production of the heart muscle and is metabolized into lactate, alanine and CO_2/HCO_3^-. It has been possible to monitor pyruvate metabolism in the heart during an ischemic episode induced in a pig, which was examined by ^{13}C chemical shift imaging following intravenous injection of hyperpolarized C_1-^{13}C pyruvate. Changes in the concentrations of these metabolites within a minute after injection were detected and metabolic maps were constructed using ^{13}C hyperpolarization-enhanced MRI. The pyruvate levels report tissue perfusion, those of alanine or lactate report cell transport, while bicarbonate reflects mitochondrial activity. After a 15 min occlusion (area of risk, but no infarct) the bicarbonate signal level in the affected area was reduced compared with that in the normal myocardium, while the alanine signal level was normal. After a 45 min occlusion (infarction) the bicarbonate signal was almost absent and the alanine signal was reduced.

5. CONCLUDING REMARKS

There are many different ways of classifying MR CAs. In this review we decided to classify those currently available using a combination of several related criteria; on the one hand, the chemical composition (metal and ligands), the magnetic properties and the effects on the MRI image, and, on the other hand, their applications resulting from their *in vivo* biodistribution. Gd^{3+} chelates are present in most types of CAs, reflecting their important role in the development of clinical applications of MRI, even adding relevant physiological information to the very high anatomical resolution characteristic of this imaging modality. Important new classes of CAs emerging are those useful in the field of molecular imaging, where the competition with other imaging modalities is less favorable. Here, nanosystems may play an important role. The need for efficient CAs at fields higher than 3 T is also a clear indication that clinical imagers seem to be quite well established. Finally, the development of hyperpolarized systems has opened up new opportunities for molecular imaging using MRI, allowing *in vivo* mapping of molecules. In particular, the use of hyperpolarized ^{13}C-labeled compounds as tracers in molecular imaging combines the high sensitivity of PET with the chemical information present in the NMR chemical shift in an unsurpassed way.

Acknowledgements

The authors thank Professor Robert N. Muller and Professor Luce Vander Elst for helpful discussions during preparation of the manuscript. This work was supported by the Foundation of Science and Technology (FCT), Portugal (project PTDC/QUI/70063/2006), FEDER, by the FNRS and the ARC Program 05/10-335 of the French Community of Belgium. It was carried out in the framework of COST Action D38 'Metal-based Systems for Molecular Imaging Applications' and EU-FP6 'Network of Excellence' EMIL (no. LSHC-2004-503569) project.

REFERENCES

1. Mansson S, Bjørnerud A. Physical principles of medical imaging by nuclear magnetic resonance. In The Chemistry of Contrast Agents in Medical Magnetic Resonance Imaging, Merbach AE, Tóth E (eds). Wiley: Chichester, 2001; 1–44.
2. Chan KW-Y, Wong W-T. Small molecular gadolinium(III) complexes as MRI contrast agents for diagnostic imaging. Coord. Chem. Rev. 2007; 251: 2428–2451.
3. Caravan P, Ellison JJ, McMurry TJ, Lauffer RB. Gadolinium(III) chelates as MRI contrast agents: structure, dynamics, and applications. Chem. Rev. 1999; 99: 2293–2352.
4. Laurent S, Vander Elst L, Muller RN. Comparative study of the physicochemical properties of six clinical low molecular weight gadolinium contrast agents. Contrast Med. Mol. Imag. 2006; 1(3): 128–137.
5. Toth E, Helm L, Merbach AE. Relaxivity of MRI contrast agents. Top. Curr. Chem. 2002; 221: 61–221.
6. Jacques V, Desreux JF. New classes of MRI contrast agents. Top. Curr. Chem. 2002; 221: 123–164.
7. Aime S, Botta M, Terreno E. Gd(III)-based contrast agents for MRI. Adv. Inorg. Chem. 2005; 57: 173–237.
8. Muller RN, Vander Elst L, Roch A, Peters JA, Csajbók E, Gillis P, Gossuin Y. Relaxation by metal-containing nanosystems. Adv. Inorg. Chem. 2005; 57: 239–292.
9. Aime S, Geninatti Crich S, Gianolio E, Giovenzana GB, Teia L, Terreno E. High sensitivity lanthanide(III) based probes for MR-medical imaging. Coord. Chem. Rev. 2006; 250: 1562–1579.
10. Yablonsky DA, Haacke EM. Theory of NMR signal behavior in magnetically inhomogeneous tissues. The static dephasing regime. Magn. Reson. Med. 1994; 32: 749–763.
11. Koenig SH, Brown RD. Field-cycling relaxometry of protein solutions and tissue: implication for MRI. Prog. Nucl. Magn. Reson. Spectr. 1990; 22: 487–567.
12. Banci L, Bertini I, Luchinat C. Nuclear and Electronic Relaxation. VCH: Weinheim, 1991.
13. Laurent S, Forge D, Port M, Roch A, Robic C, Vander Elst L, Muller RN. Magnetic iron oxide nanoparticles: synthesis, stabilization, vectorization, physico-chemical characterizations and biological applications. Chem. Rev. 2008; 108(6): 2064–2110.
14. Gueron M. Nuclear relaxation in macromolecules by paramagnetic ions: a novel mechanism. J. Magn. Reson. 1975; 19: 58–66.
15. Gillis P, Koenig SH. Transverse relaxation of solvent protons induced by magnetized spheres: application to ferritin, erythrocytes and magnetite. Magn. Reson. Med. 1987; 5: 323–345.
16. Freed JH. Dynamic effects of pair correlation functions on spin relaxation by translational diffusion in liquids. II. Finite jumps and independent T_1 processes. J. Chem. Phys. 1978; 68: 4034–4037.
17. Koenig SH, Kellar KE. Theory of $1/T_1$ and $1/T_2$ NMRD profiles of solutions of magnetic nanoparticles. Magn. Reson. Med. 1995; 34: 227–233.
18. Roch A, Muller RN, Gillis P. Theory of proton relaxation induced by superparamagnetic particles. J. Chem. Phys. 1999; 110: 5403–5411.
19. Vogl TJ, Hammerstingl R, Schwarz W, Mack MG, Muller PK, Pegios W, Keck H, Eibl-Eibesfeldt A, Hoelzl J, Woessmer B, Bergman C, Felix R. Superparamagnetic iron oxide enhanced versus gadolinium-enhanced MR imaging for differential diagnosis of focal liver lesions. Radiology 1996; 198: 881–887.
20. Keller KE, Fujii DK, Gunther WHH, Briely-Sæbø K, Bjørnesud A, Spiller M, Koenig SH. NC100150 injection, a preparation of optimized iron oxide nanoparticles for positive-contrast MR angiography. J. Magn. Reson. Imag. 2000; 11: 488–494.
21. Ahlström KH, Johansson LO, Rodenburg JB, Ragnarsson AS, Åkeson P, Børseth A. Pulmonary MR angiography with ultrasmall superparamagnetic iron oxide particles as a blood pool agent and a navigator echo for respiratory gating: pilot study. Radiology 1999; 211: 865–869.

22. Jung CW, Jacobs P. Physical and chemical properties of superparamagnetic iron oxide MR contrast agents: ferumoxides, ferumoxtran, ferumoxsil. Magn. Reson. Imag. 1995; 13: 661–674.
23. Bachmann R, Conrad R, Kreft B, Luzar O, Block W, Flacke S, Pauleit D, Träber F, Gieseke J, Saebo K, Schild H. Evaluation of a new ultrasmall superparamagnetic iron oxide contrast agent Clariscan, (NC100150) for MRI of renal perfusion: experimental study in an animal model. J. Magn. Reson. Imag. 2002; 16: 190–195.
24. Groma EV, Josephson L, Lewis JM. US Patent 4827945, 1989.
25. Reimer P, Müller M, Marx C, Weidermann D, Muller RN, Rummeny EJ, Ebert W, Shamsi K, Peters PE. T_1 effects of a bolus-injectable superparamagnetic iron oxide, SH U 555A: dependence on field strength and plasma concentration—preliminary clinical experience with dynamic T_1-weighted MR imaging. Radiology 1998; 209: 831–836.
26. Bremer C, Alkemper T, Baermig J, Reimer P. Contrast-enhanced 3D-MRA of the upper abdomen with a bolus-injectable SPIO (SH U 555 A). J. Magn. Reson. Imag. 1999; 10: 65–71.
27. Jacobson T, Klaveness J. PCT Int. Appl. WO 00017, 1985.
28. Rinck PA, Smevik O, Nilsen G, Klepp O, Onsrud M, Øksendal A, Borseth A. Oral magnetic particles in MR imaging of the abdomen and pelvis. Radiology 1991; 178: 775–779.
29. Prasad PV, Edelman RR, Epstein FH. Non-invasive evaluation of intra-renal oxygenation using BOLD MRI. Circulation 1996; 94: 3271–3275.
30. Van Wagoner M, Worah D. Gadodiamide injection. First human experience with the nonionic magnetic resonance imaging enhancement agent. Invest. Radiol. 1993; 28: S44–S48.
31. Oskendal A, Hals P. Biodistribution and toxicity of MR imaging contrast media. J. Magn. Reson. Imag. 1993; 3: 157–165.
32. Bellin M-F, Vasile M, Morel-Precetti S. Currently used non-specific extracellular MR contrast media. Eur. Radiol. 2003; 13: 2688–2698.
33. Bellin M-F. MR contrast agents, the old and the new. Eur. J. Radiol. 2006; 60: 314–323.
34. Grobner T. Gadolinium: a specific trigger for the development of nephrogenic fibrosing dermopathy and nephrogenic systemic fibrosis? Nephrol. Dial. Transplant. 2006; 21: 1104–1108.
35. Ersoy H, Rybicki FJ. Biochemical safety profiles of gadolinium-based extracellular contrast agents and nephrogenic systemic fibrosis. J. Magn. Reson. Imag. 2007; 26: 1190–1197.
36. Rofsky NM, Sherry AD, Lenkinsky RE. Nephrogenic systemic fibrosis: a chemical and rational perspective. Radiology 2008; 247: 608–612.
37. Knopp MV, von Tengg-Koblingk H, Floemer F, Schoenberg SO. Contrast agents for MRA: future directions. J. Magn. Reson. Imag. 1999; 10: 314–331.
38. Saeed M, Wendland MF, Higgins CB. Blood pool contrast agents for cardiovascular imaging. J. Magn. Reson. Imag. 2001; 12: 890–898.
39. Daldrup-Link H, Brasch RC. Macromolecular contrast agents for MR mammography: current status. Eur. Radiol. 2003; 13: 354–365.
40. Aime S, Botta M, Fasano M, Crich SG, Terreno E. Gd(III) complexes as contrast agents for magnetic resonance imaging: a proton relaxation enhancement study of the interaction with human serum albumin. J. Biol. Inorg. Chem. 1996; 1: 312–319.
41. Lauffer RB, Parmelee DJ, Dunham SU, Ouellet HS, Dolan RP, Witte S, McMurry TJ, Walovitch RC. MS-325: albumin-targeted contrast agent for MR angiography. Radiology 1998; 207: 529–538.
42. Rohrer M, Bauer H, Mintorovitch J, Requardt M, Weinmann H-J. Comparison of magnetic properties of MRI contrast media solutions at different magnetic field strengths. Invest. Radiol. 2005; 40: 715–724.
43. Cavagna FM, Lorusso V, Anelli PL, Maggioni F, de Haën C. Preclinical profile and clinical potential of gadocoletic acid trisodium salt (B22956/1), a new intravascular contrast medium for MRI. Acad. Radiol. 2002; 9: 491–494.
44. Preda A, Novikov V, Möglich M, Turetschek K, Shames DM, Brasch RC, Cavagna FM, Roberts TPL. MRI monitoring of Avastin antiangiogenesis therapy using B22956/1, a new blood pool contrast agent, in an experimental model of human cancer. J. Magn. Reson. Imag. 2004; 20: 865–873.
45. Dong Q, Hurst DR, Weinmann HJ, Chenevert TJ, Londy FJ, Prince MR. Magnetic resonance angiography with Gadomer-17. An animal study original investigation. Invest. Radiol. 1998; 33: 699–708.
46. Misselwitz B, Schmitt-Willich H, Ebert W, Frenzel T, Weinmann HJ. Pharmacokinetics of Gadomer-17, a new dendritic magnetic resonance contrast agent. MAGMA 2001; 12: 128–134.
47. Kobayashi H, Brechbiel MW. Dendrimer-based nanosized MRI contrast agents. Curr. Pharm. Biotechnol. 2004; 5: 539–549.
48. Aime S, Fasano M, Terreno E, Botta M. Protein-bound metal chelates. In The Chemistry of Contrast Agents in Medical Magnetic Resonance Imaging, Merbach AE, Tóth E (eds). Wiley: Chichester, 2001; 193–241.
49. Berthezène Y, Vexler V, Price DC, Wisner-Dupon J, Moseley ME, Aicher KP, Brasch RC. Magnetic resonance imaging detection of an experimental pulmonary perfusion deficit using a macromolecular contrast agent. Polylysine-gadolinium-DTPA40. Invest. Radiol. 1992; 27: 346–351.
50. Sieving PF, Watson AD, Rocklage SM. Preparation and characterization of paramagnetic polychelates and their protein conjugates. Bioconjug. Chem. 1990; 1: 65–71.
51. Aime S, Botta M, Crich SG, Giovenzana G, Palmisano G, Sisti M. Novel paramagnetic macromolecular complexes derived from the linkage of a macrocyclic Gd(III) complex to polyamino acids through a squaric acid moiety. Bioconjug. Chem. 1999; 10: 192–199.
52. Curtet C, Maton F, Havet T, Slinkin M, Mishra A, Chatal JF, Muller RN. Polylysine-Gd-DTPA(*n*) and polylysine-Gd-DOTA(*n*) coupled to anti-CEA F(ab ')(2) fragments as potential immunocontrast agents—relaxometry, biodistribution, and magnetic resonance imaging in nude mice grafted with human colorectal carcinoma. Invest. Radiol. 1998; 33: 752–761.
53. Wu C, Brechbiel W, Kozak RW, Gansow OA. Metal–chelate–dendrimer–antibody constructs for use in radioimmunotherapy and imaging. Bioorg. Med. Chem. Lett. 1994; 4: 449–454.
54. Lu ZR, Parker DL, Goodrich KC, Wang X, Dalle JG, Buswell HR. Extracellular biodegradable macromolecular gadolinium(III) complexes for MRI. Magn. Reson. Med. 2004; 51: 27–34.
55. Corot C, Violas X, Robert P, Gagneur G, Port M. Comparison of different types of blood pool agents (P792, MS325, USPIO) in a rabbit MR angiography-like protocol. Invest. Radiol. 2003; 38: 311–319.
56. Lokling KE, Fossheim SL, Skurtveit R, Bjornerud A, Klaveness J. pH-sensitive paramagnetic liposomes as MRI contrast agents: *in vitro* feasibility studies. Magn. Reson. Imag. 2001; 19: 731–738.
57. Weissleder R, Elizondo G, Wittenberg J, Rabito CA, Bengele HH, Josephson L. Ultrasmall superparamagnetic iron oxide: characterization of a new class of contrast agents for MR imaging. Radiology 1990; 175: 489–493.
58. Weinmann HJ, Bauer H, Ebert W, Frenzel T, Radüchel B, Platzek J, Schmitt-Willich H. Comparative studies on the efficacy of MRI contrast agents in MRA. Acad. Radiol. 2002; (Suppl. 1): S135–6.
59. Taupitz M, Schnorr J, Abramjuk C, Wagner S, Pilgrimm H, Hünigen H, Hamm B. New generation of monomer-stabilized very small superparamagnetic iron oxide particles (VSOP) as contrast medium for mr angiography: preclinical results in rats and rabbits. J. Magn. Reson. Imag. 2000; 12: 905–911.
60. Mornet S, Vasseur S, Grasset F, Duguet E. Magnetic nanoparticle design for medical diagnosis and therapy. J. Mater. Chem. 2004; 14: 2164–2175.
61. Mack MG, Balzer JO, Straub R, Eichler K, Vogl TJ. Superparamagnetic iron oxide-enhanced MR imaging of head and neck lymph nodes. Radiology 2002; 222: 239–244.
62. Schmitt-Willich H, Brehm M, Evers CLJ, Michl G, Muller-Fahrnow A, Petrov O, Platzek J, Raduchel B, Sulzle D. Synthesis and physicochemical characterization of a new gadolinium chelate: the liver-specific magnetic resonance imaging contrast agent Gd–EOB–DTPA. Inorg. Chem. 1999; 38: 1134–1144.
63. Schuhmann-Giampieri G, Schmitt-Willich H, Press WR, Negishi C, Weinmann HJ, Speck U. Preclinical evaluation of Gd–EOB–DTPA as a contrast agent in MR imaging of the hepatobiliary system. Radiology 1992; 183: 59–64.

64. Uggeri F, Aime S, Anelli PL, Botta M, Brocchetta M, Dehaen C, Ermondi G, Grandi M, Paoli P. Novel contrast agents for magnetic resonance imaging. Synthesis and characterization of the ligand BOPTA and its Ln(III) complexes (Ln=Gd, La, Lu). X-ray structure of disodium (TPS-9–145337286-C-S)-[4-Carboxy-5,8,11-tris(carboxymethyl)-1-phenyl-2-oxa-5,8,11-triaza tridecan-13-oato(5-)]gadolinate(2-) in a mixture with its enantiomer. Inorg. Chem. 1995; 34: 663–642.
65. Henrotte V, Vander Elst L, Laurent S, Muller RN. Comprehensive investigation of the non-covalent binding of MRI contrast agents with human serum albumin. J. Biol. Inorg. Chem. 2007; 12: 929–937.
66. Knopp MV, Schoenberg SO, Rehm C, Floemer F, von Teregg-Kobling KH, Bock M, Hentrich HR. Assessment of gadobenate dimeglumine for magnetic resonance angiography: Phase I studies. Invest. Radiol. 2002; 37: 706–715.
67. Saini S, Nelson RC. Technique for MR imaging of the liver. Radiology 1995; 197: 575–577.
68. Lim KO, Stark DD, Leese PT, Pfefferbaum A, Rocklage SM, Quay SC. Hepatobiliary MR imaging: first human experience with MnDPDP. Radiology 1991; 178: 79–82.
69. Reimer P, Rummeny EJ, Daldrup HE, Balzer T, Tombach B, Berns T, Peters PE. Clinical results with Resovist: a phase 2 clinical trial. Radiology 1995; 195: 489–496.
70. Hamm B, Thoeni RF, Gould RG, Bernardino ME, Luning M, Saini S, Mahfouz AE, Taupitz M, Wolf KJ. Focal liver lesions: characterization with nonenhanced and dynamic contrast material-enhanced MR imaging. Radiology 1994; 190: 417–423.
71. Misselwitz B, Platzek J, Radüchel B, Oellinger JJ, Weinmann H-J. Gadofluorine 8: initial experience with a new contrast medium for interstitial MR lymphography. MAGMA 1999; 8: 1352–8661.
72. Silva AC, Lee JH, Aoki I, Koretsky AP. Manganese-enhanced magnetic resonance imaging (MEMRI): methodological and practical considerations. NMR Biomed. 2004; 17: 532–543.
73. Watanabe T, Tammer R, Boretius S, Frahm J, Michaelis T. Chromium(VI) as a novel MRI contrast agent for cerebral white matter—preliminary results in mouse brain *in vivo*. Magn. Reson. Med. 2006; 56: 1–6.
74. Poduslo JF, Wengenack TM, Curran GL, Wisniewski T, Sigurdsson EM, Macura SI, Borowski BJ, Jack CR. Molecular targeting of Alzheimer's amyloid plaques for contrast-enhanced magnetic resonance imaging. Neurobiol. Dis. 2002; 11: 315–329.
75. Wadghiri YZ, Sigurdsson EM, Sadowski M, Elliott JI, Li YS, Scholtzova H, Tang CY, Aguinaldo G, Pappolla M, Duff K, Wisniewski T, Turnbull DH. Detection of Alzheimer's amyloid in transgenic mice using magnetic resonance microimaging. Magn. Reson. Med. 2003; 50: 293–302.
76. Takahara T, Saeki M, Nosaka S. Nippon Igaku Hoshasen Gakkai Zasshi. 1995; 55: 697–699.
77. Rubin DL, Falk KL, Sperling MJ, Ross M, Saini S, Rothman B, Shellock F, Zerhouni E, Stark D, Outwater EK, Schmiedl U, Kirby LC, Chezmar J, Coates T, Chang M, Silverman JM, Rofsky N, Burnett K, Engel J, Young SW. A multicenter clinical trial of Gadolite Oral Suspension as a contrast agent for MRI. J. Magn. Reson. Imag. 1997; 7: 865–872.
78. Lonnemark M, Hemmingsson A, Carlsten J, Ericsson A, Holtz E, Klaveness J. Superparamagnetic particles as an MRI contrast agent for the gastrointestinal tract. Acta Radiol. 1988; 29: 599–602.
79. Bogdanov AA, Lewin M, Weissleder R. Approaches and agents for imaging the vascular system. Adv. Drug Deliv. Rev. 1999; 37: 279–293.
80. Nunn AD, Linder KE, Tweedle MF. Can receptors be imaged with MRI agents? Q.J. Nucl. Med. 1997; 41: 155–162.
81. Aime S, Botta M, Garino E, Crich SG, Giovenzana G, Pagliarin R, Palmisano G, Sisti M. Non-covalent conjugates between cationic polyamino acids and Gd^{III} chelates: a route for seeking accumulation of MRI-contrast agents at tumor targeting sites. Chem. Eur. J. 2000; 6: 2609–2617.
82. Frullano L, Rohovec J, Aime S, Maschmeyer T, Prata MIM, de Lima JJP, Geraldes CFGC, Peters JA. Towards targeted MRI: new MRI contrast agents for sialic acid detection. Chem. Eur. J. 2004; 10: 5205–5217.
83. Young SW, Quing F, Harriman A, Sessler JL, Dow WC, Mody TD, Hemmi GW, Hao Y, Miller RA. Gadolinium(III) texaphyrin: A tumor selective radiation sensitizer that is detectable by MRI. Proc. Natl Acad. Sci. USA. 1996; 93: 6610–6615.
84. Ni Y, Pislaru C, Bosmans H, Pislaru S, Miao Y, Bogaert J, Dymarkowski S, Yu J, Semmler W, Van de Werf F, Baert AL, Marchal G. Intracoronary delivery of Gd-DTPA and Gadophrin-2 for determination of myocardial viability with MR imaging. Eur. Radiol. 2001; 11: 876–883.
85. Sipkins DA, Cheresh DA, Kazemi MR, Nevin LM, Bednarski MD, Li KC. Detection of tumor angiogenesis *in vivo* by alphaVbeta3-targeted magnetic resonance imaging. Nat. Med. 1998; 4: 623–626.
86. Winter PM, Caruthers SD, Kassner A, Harris TD, Chinen LK, Allen JS, Lacy EK, Zhang H, Robertson JD, Wickline SA, Lanza GM. Molecular imaging of angiogenesis in nascent Vx-2 rabbit tumors using a novel $\alpha_v\beta_3$-targeted nanoparticle and 1.5 Tesla magnetic resonance imaging. Cancer Res. 2003; 63: 5838–5843.
87. Aime S, Cabella C, Colombatto S, Geninatti Crich S, Gianolio E, Maggioni F. Insights into the use of paramagnetic Gd(III) complexes in MR-molecular imaging investigations. J. Magn. Reson. Imag. 2002; 16: 394–406.
88. Crich SG, Biancone L, Cantaluppi V, Duo D, Esposito G, Russo S, Camussi G, Aime S. Improved route for the visualization of stem cells labeled with a Gd-/Eu-chelate as dual (MRI and fluorescence) agent. Magn. Reson. Med. 2004; 51: 938–944.
89. Aime S, Frullano L, Crich SG. Compartmentalization of a gadolinium complex in the apoferritin cavity: a route to obtain high relaxivity contrast agents for magnetic resonance imaging. Angew. Chem. Int. Edn Engl. 2002; 41: 1017–1019.
90. Terreno E, Crich SG, Belfiore S, Biancone L, Cabella C, Esposito G, Manazza AD, Aime S. Effect of the intracellular localization of a Gd-based imaging probe on the relaxation enhancement of water protons. Magn. Reson. Med. 2006; 55: 491–497.
91. Bhorade R, Weissleder R, Nakakoshi T, Moore A, Tung CH. Macrocyclic chelators with paramagnetic cations are internalized into mammalian cells via a HIV-tat derived membrane translocation peptide. Bioconjug. Chem. 2000; 11: 301–305.
92. Heckl S, Pipkorn R, Waldeck W, Spring H, Jenne J, von der Lieth CW, Corban-Wilhelm H, Debus J, Braun K. Intracellular visualization of prostate cancer using magnetic resonance imaging. Cancer Res. 2003; 63: 4766–4772.
93. Kalman FK, Woods M, Caravan P, Jurek P, Spiller M, Tircsó G, Kiraly R, Brücher E, Sherry AD. Potentiometric and relaxometric properties of a gadolinium-based MRI contrast agent for sensing tissue pH. Inorg. Chem. 2007; 46: 5260–5270.
94. Aime S, Crich SG, Gianolio E, Tei L, Terreno E. High sensitivity lanthanide(III) based probes for MR-medical imaging. Coord. Chem. Rev. 2006; 250: 1562–1579.
95. Zhang S, Wu K, Sherry AD. A novel pH-sensitive MRI contrast agent. Angew. Chem. Int. Edn Engl. 1999; 38: 3192–3194.
96. Raghunand N, Howison C, Sherry AD, Zhang S, Gillies R. Renal and systemic pH imaging by contrast-enhanced MRI. Magn. Reson. Med. 2003; 49: 249–257.
97. Garcia-Martin ML, Martinez GV, Raghunand N, Sherry AD, Zhang S, Gillies R. High resolution pH_e imaging of rat glioma using pH-dependent relaxivity. Magn. Reson. Med. 2006; 55: 309–315.
98. Mikawa M, Miwa N, Brautigam M, Akaike T, Maruyama A. A pH-sensitive contrast agent for functional magnetic resonance imaging (MRI). Chem. Lett. 1998; 7: 693–694.
99. Aime S, Crich SG, Botta M, Giovenzana G, Palmisano G, Sisti M. A macromolecular Gd(III) complex as pH-responsive relaxometric probe for MRI applications. Chem. Commun. 1999; 1577–1578.
100. Lowe MP, Parker D, Reany O, Aime S, Botta M, Castellano G, Gianolio E, Pagliarin R. pH-dependent modulation of relaxivity and luminescence in macrocyclic gadolinium and europium complexes based on reversible intramolecular sulfonamide ligation. J. Am. Chem. Soc. 2001; 123: 7601–7609.
101. Hovland R, Glogard C, Aasen AJ, Klaveness J. Gadolinium DO3A derivatives mimicking phospholipids; preparation and *in vitro* evaluation as pH responsive MRI contrast agents. J. Chem. Soc. Perkin Trans. 2 2001; 6: 929–933.
102. Woods M, Zhang S, Ebron VH, Sherry AD. PH-sensitive modulation of the second hydration sphere in Lanthanide(III) tetraamide–DOTA complexes: a novel approach to smart MR contrast media. Chem. Eur. J. 2003; 9: 4634–4640.

103. Aime S, Barge A, Botta M, Howard JAK, Kataly R, Lowe MP, Moloney JM, Parker D, de Sousa AS. Dependence of the relaxivity and luminescence of gadolinium and europium amino-acid complexes on hydrogencarbonate and pH. Chem. Commun. 1999; 1047–1048.
104. Toth E, Bolskar RD, Borel A, Gonzalez G, Helm L, Merbach AE, Sitharaman B, Wilson LJ. Water-soluble gadofullerenes: toward high-relaxivity, pH-responsive MRI contrast agents. J. Am. Chem. Soc. 2005; 127: 799–805.
105. Aime S, Botta M, Fasano M, Terreno E, Kinchesh P, Calabi L, Paleari L. A new ytterbium chelate as contrast agent in chemical shift imaging and temperature sensitive probe for MR spectroscopy. Magn. Reson. Chem. 1996; 35: 648–651.
106. Zuo CS, Mahmood A, Sherry AD. TmDOTA(−): a sensitive probe for MR thermometry *in vivo*. J. Magn. Reson. 2001; 151: 101–106.
107. Fossheim SL, Il'yasov KA, Hennig J, Bjornerud A. Thermosensitive paramagnetic liposomes for temperature control during MR imaging-guided hyperthermia: *in vitro* feasibility studies. Acad. Radiol. 2000; 7: 1107–1115.
108. Thulborn KR, Waterton JC, Matthews PM, Radda GK. Oxygenation dependence of the transverse relaxation time of water protons in whole blood at high field. Biochem. Biophys. Acta 1982; 714: 265–270.
109. Ogawa S, Tank DW, Menon R, Ellermann JM, Kim SG, Merkle H, Ugurbil K. Intrinsic signal changes accompanying sensory stimulation: functional brain mapping with magnetic resonance imaging. Proc. Natl Acad. Sci. USA 1992; 89: 5951–5955.
110. Burai L, Scopelliti R, Toth E. Eu-II-cryptate with optimal water exchange and electronic relaxation: a synthon for potential pO(2) responsive macromolecular MRI contrast agents. Chem. Commun. 2002; 20: 2366–2367.
111. Aime S, Botta M, Gianolio E, Terreno E. A p(O-2)-responsive MRI contrast agent based on the redox switch of manganese(II/III)–porphyrin complexes. Angew. Chem. Int. Edn Engl. 2000; 39: 747–750.
112. Louie AY, Huber MM, Ahrens ET, Rothbacher U, Moats R, Jacobs RE, Fraser SE, Meade TJ. In vivo visualization of gene expression using magnetic resonance imaging. Nat. Biotechnol. 2000; 18: 321–325.
113. Himmelreich U, Aime S, Hieronymus T, Justicia C, Uggeri F, Zenke M, Hoehn M. A responsive MRI contrast agent to monitor functional cell status. Neuroimage 2006; 32: 1142–1149.
114. Anelli PL, Bertini I, Fragai M, Lattuada L, Luchinat C, Parigi G. Sulfonamide-functionalized gadolinium DTPA complexes as possible contrast agents for MRI: a relaxometric investigation. Eur. J. Inorg. Chem. 2000; 625–630.
115. Nivorozhkin AL, Kolodziej AF, Caravan P, Greenfield MT, Lauffer RB, Mc Murry TJ. Enzyme-activated Gd^{3+} magnetic resonance imaging contrast agents with a prominent receptor-induced magnetization enhancement. Angew. Chem. Int. Edn 2001; 40: 2903–2906.
116. Bogdanov A, Matuszewski L, Bremer C, Petrovsky A, Weissleder R. Oligomerization of paramagnetic substrates result in signal amplification and can be used for MR imaging of molecular targets. Mol. Imag. 2002; 1: 16–23.
117. Duimstra JA, Femia FJ, Meade TM. A gadolinium chelate for detection of beta-glucuronidase: a self-immolative approach. J. Am. Chem. Soc. 2005; 127: 12847–12855.
118. Querol M, Chen JW, Weissleder R, Bogdanov A. DTPA-bisamide-based MR sensor agents for peroxidase imaging. Org. Lett. 2005; 7: 1719–1722.
119. Chen JW, Pham W, Weissleder R, Bogdanov A. Human myeloperoxidase: a potential target for molecular MR imaging in atherosclerosis. Magn. Reson. Med. 2004; 52(5): 1021–1028.
120. Li W-H, Parigi G, Fragai M, Luchinat C, Meade TJ. Mechanistic studies of a calcium-dependent MRI contrast agent. Inorg. Chem. 2002; 41: 4018–4024.
121. Li W-H, Fraser SE, Meade TJ. A calcium-sensitive magnetic resonance imaging contrast agent. J. Am. Chem. Soc. 1999; 121: 1413–1414.
122. Hanaoka K, Kikuchi K, Urano Y, Nagano T. Selective sensing of zinc ions with a novel magnetic resonance imaging contrast agent. J. Chem. Soc Perkin Trans. 1 2001; 2: 1840–1843.
123. Hanaoka K, Kikuchi K, Urano Y, Narazaki M, Yokawa T, Sakamoto S, Yamaguchi K, Nagano T. Design and synthesis of a novel magnetic resonance imaging contrast agent for selective sensing of zinc ion. Chem. Biol. 2002; 9: 1027–1032.
124. Aime S, Botta M, Fasano M, Terreno E. Gd(III)–Fe(III) heterobimetallic complexes of DTPA-bis-salicylamide. Spectrochim. Acta. 1993; 49A: 1315–1322.
125. Comblin V, Gilsoul D, Hermann M, Humblet V, Jacques V, Mesbahi M, Sauvage C, Desreux JF. Designing new MRI contrast agents: a coordination chemistry challenge. Coord. Chem. Rev. 1999; 185–186: 451–470.
126. Paris J, Gameiro C, Humblet V, Mohapatra PK, Jacques V, Desreux JF. Auto-assembling of ditopic macrocyclic lanthanide chelates with transition-metal ions. Rigid multimetallic high relaxivity contrast agents for magnetic resonance imaging. Inorg. Chem. 2006; 45: 5092–5102.
127. Costa J, Ruloff R, Burai L, Helm L, Merbach AE. Rigid (ML2Gd2III)-L-II (M=Fe, Ru) complexes of a terpyridine-based heteroditopic chelate: A class of candidates for MRI contrast agents. J. Am. Chem. Soc. 2005; 127: 5147–5157.
128. Livramento JB, Weidensteiner C, Prata MIM, Allegrini PR, Geraldes CFGC, Helm L, Kneuer R, Merbach AE, Santos AC, Schmidt P, Tóth E. First *in vivo* MRI assessment of a self-assembled metallostar compound endowed with a remarkable high field relaxivity. Contrast Med. Mol. Imag. 2006; 1: 30–39.
129. Parac-Vogt TN, Vander Elst L, Kimpe K, Laurent S, Burtéa C, Chen F, Van Deun R, Ni Y, Muller RN, Binnemans K. Pharmacokinetic and *in vivo* evaluation of a self-assembled gadolinium(III)-iron(II) contrast agent with high relaxivity. Contrast Med. Mol. Imag. 2006; 1: 267–278.
130. Gløgård C, Stensrud G, Aime S. Novel radical-responsive MRI contrast agent based on paramagnetic liposomes. Magn. Reson. Chem. 2003; 41: 585–588.
131. Ward KM, Aletras AH, Balaban RS. A new class of contrast agents for MRI based on proton chemical exchange dependent saturation transfer (CEST). J. Magn. Reson. 2000; 143: 79–87.
132. Zhou J, Wilson DA, Sun PZ, Klaus JA, van Zijl PC. Quantitative description of proton exchange processes between water and endogenous and exogenous agents for WEX, CEST, and APT experiments. Magn. Reson. Med. 2004; 51: 945–952.
133. Guivel-Scharen V, Sinnwell T, Wolff SD, Balaban RS. Detection of proton chemical exchange between metabolites and water in biological tissues. J. Magn. Reson. 1998; 133: 36–45.
134. Zhang S, Winter P, Wu K, Sherry AD. A novel europium(III)-based MRI contrast agent. J. Am. Chem. Soc. 2001; 123: 1517–1518.
135. Zhang S, Merritt M, Woessner DE, Lenkinski RE, Sherry AD. PARACEST agents: modulating MRI contrast via water proton exchange. Acc. Chem. Res. 2003; 36: 783–790.
136. Aime S, Carrera C, Castelli DD, Crich SG, Terreno E. Tunable imaging of cells labeled with MRI-PARACEST agents. Angew. Chem. Int. Edn Engl. 2005; 44: 1813–1815.
137. Aime S, Castelli DD, Terreno E. Novel pH-reporter MRI contrast agents. Angew. Chem. Int. Edn Engl. 2002; 41: 4334–4336.
138. Aime S, Barge A, Castelli DD, Fedeli F, Mortillaro A, Nielsen FU, Terreno E. Paramagnetic lanthanide(III) complexes as pH-sensitive chemical exchange saturation transfer (CEST) contrast agents for MRI applications. Magn. Reson. Chem. 2002; 47: 639–648.
139. Zhang S, Michaudet L, Burgess S, Sherry AD. The amide protons of an ytterbium(III) dota tetraamide complex act as efficient antennae for transfer of magnetization to bulk water. Angew. Chem. Int. Edn Engl. 2002; 41: 1919–1921.
140. Aime S, Castelli DD, Terreno E. A paramagnetic MRI-CEST agent responsive to lactate concentration. J. Am. Chem. Soc. 2002; 124: 9364–9365.
141. Aime S, Castelli DD, Terreno E. Supramolecular adducts between poly-L-arginine and [Tm(III)dotp]: a route to sensitivity-enhanced magnetic resonance imaging-chemical exchange saturation transfer agents. Angew. Chem. Int. Edn Engl. 2003; 42: 4527–4529.
142. Zhang S, Trokowski R, Sherry AD. A paramagnetic CEST agent for imaging glucose by MRI. J. Am. Chem. Soc. 2003; 125: 15288–15289.
143. Trokowski R, Ren J, Kalman FK, Sherry AD. Selective sensing of zinc ions with a PARACEST contrast agent. Angew. Chem. Int. Edn Engl. 2005; 44: 6920–6923.
144. Zhang S, Malloy CR, Sherry AD. MRI thermometry based on PARACEST agents. J. Am. Chem. Soc. 2005; 127: 17572–17573.

145. Yoo B, Pagel MD. A PARACEST MRI contrast agent to detect enzyme activity. J. Am. Chem. Soc. 2006; 128: 14032–14033.
146. Woods M, Woessner DE, Sherry AD. Paramagnetic lanthanide complexes as PARACEST agents for medical imaging. Chem. Soc. Rev. 2006; 35: 500–511.
147. Terreno E, Castelli DD, Cravotto G, Milone L, Aime S. Ln(III)-DOTAMGIY complexes: a versatile series to assess the determinants of the efficacy of paramagnetic chemical exchange saturation transfer agents for magnetic resonance imaging applications. Invest. Radiol. 2004; 39: 235–243.
148. Goffeney N, Bulte JW, Duyn J, Bryant LH, van Zijl PC. Sensitive NMR detection of cationic-polymer-based gene delivery systems using saturation transfer via proton exchange. J. Am. Chem. Soc. 2001; 123: 8628–8629.
149. Snoussi K, Bulte JW, Gueron M, van Zijl PC. Sensitive CEST agents based on nucleic acid imino proton exchange: Detection of poly(rU) and of a dendrimer-poly(rU) model for nucleic acid delivery and pharmacology. Magn. Reson. Med. 2003; 49: 998–1005.
150. Aime S, Castelli DD, Terreno E. Highly sensitive MRI chemical exchange saturation transfer agents using liposomes. Angew. Chem. Int. Edn Engl. 2005; 44: 5513–5515.
151. Winter PM, Cai K, Chen J, Adair CR, Kiefer GE, Athey PS, Gaffney PJ, Buff CE, Robertson JD, Caruthers SD, Wickline SA, Lanza GM. Targeted PARACEST nanoparticle contrast agent for the detection of fibrin. Magn. Reson. Med. 2006; 56: 1384–1388.
152. Mansson S, Johansson E, Magnusson P, Chai CM, Hansson G, Petersson JS, Stahlberg F, Golman K. C-13 imaging—a new diagnostic platform. Eur. Radiol. 2006; 16: 57–67.
153. Golman K, Ardenkjaer-Larsen JH, Petersson JS, Mansson S, Leunbach I. Molecular imaging with endogenous substances. Proc. Natl Acad. Sci. USA. 2003; 100: 10435–10439.
154. Möller HE, Chen XJ, Saam B, Hagspiel KD, Johnson GA, Altes TA, de Lange EE, Kauczor HU. MRI of the lungs using hyperpolarized noble gases. Magn. Reson. Med. 2002; 47: 1029–1051.
155. van Heeswijk R, Laus S, Morgenthaler F, Gruetter R. Relaxivity of Gd-based contrast agents on X nuclei with long intrinsic relaxation times in aqueous solutions. Magn. Reson. Imag. 2007; 25: 821–825.
156. Bowers CR, Weitekamp DP. Para-Hydrogen and synthesis allow dramatically enhanced nuclear alignment. J. Am. Chem. Soc. 1987; 109: 5541–5542.
157. Abragam A. The Principles of Nuclear Magnetism. Clarendon Press: Oxford, 1961.
158. Johansson E, Olsson LE, Mansson S, Petersson JS, Golman K, Stahlberg F, Wirestam R. Perfusion assessment with bolus differentiation: a technique applicable to hyperpolarized tracers. Magn. Reson. Med. 2004; 52: 1043–1051.
159. Magnusson P, Johansson E, Mansson S, Petersson JS, Chai CM, Hansson G, Axelsson O, Golman K. Passive catheter tracking during interventional MRI using hyperpolarized C-13. Magn. Reson. Med. 2007; 57: 1140–1147.
160. Ardenkjaer-Larsen JH, Fridlund B, Gram A, Hansson G, Hansson L, Lerche MH, Servin R, Thaning M, Golman K. Increase in signal-to-noise ratio of >10,000 times in liquid-state NMR. Proc. Natl Acad. Sci. USA 2003; 100: 10158–10163.
161. Ishii M, Emami K, Kadlecek S, Petersson JS, Golman K, Vahdat V, Yu J, Cadman RV, MacDuffie-Woodburn J, Stephen M, Lipson DA, Rizi RR. Hyperpolarized C-13 MRI of the pulmonary vasculature and parenchyma. Magn. Reson. Med. 2007; 57: 459–463.
162. Olsson LE, Chai CM, Axelsson O, Karlsson M, Golman K, Petersson JS. MR coronary angiography in pigs with intraarterial injections of a hyperpolarized C-13 substance. Magn. Reson. Med. 2006; 55: 731–737.
163. Golman K, Zandt R, Lerche M, Pehrson R, Ardenkjaer-Larsen JH. Metabolic imaging by hyperpolarized C-13 magnetic resonance imaging for *in vivo* tumor diagnosis. *Cancer Res*. 2006; 66: 10855–10860.
164. Golman K, Petersson JS, Magnusson P, Johansson E, Åkeson P, Chai C-M, Hansson G, Månsson S. Cardiac metabolism measured noninvasively by hyperpolarized C-13 MRI. Magn. Reson. Med. 2008; 59: 1005–1013.

